PHILOSOPHICAL TRANSACTIONS OF THE ROYAL SOCIETY A MATHEMATICAL, PHYSICAL & ENGINEERING SCIENCES

Routes to Chaos and Turbulence. A Computational Introduction

John Argyris, Gunter Faust and Maria Haase

Phil. Trans. R. Soc. Lond. A 1993 **344**, 207-234
doi: 10.1098/rsta.1993.0088

Routes to chaos and turbulence. A computational introduction

By John Argyris, Gunter Faust and Maria Haase

Institute for Computer Applications, University of Stuttgart, D-7000 Stuttgart 80, Germany

[Plates 1–6]

Contents

We propose to survey in this paper different routes to chaos arising in nonlinear dynamic systems emphasizing where appropriate the connection with the intriguing phenomenon of turbulence in a viscous fluid. The onset of turbulence displays, in particular, clear chaotic characteristics. On the other hand, fully developed turbulence cannot be analysed presently by chaos theory as it stands and demands an expansion of the basic theory to incorporate spatial dependencies. Here we shall refer only to the onset of turbulence. Our approach is essentially a computational exploration and illustration.

1. Survey of the problem

For more than a hundred years, many outstanding physicists have grappled with the problem of turbulence and with the cause for the instability of flows. And yet turbulence continues, for all the formidable mathematical apparatus invested in its exploration, to be a fundamentally open problem in physics; we still lack convincing physical models and associated computational schemes to predict with technical precision turbulent behaviour.

From its initiation, the philosophical framework of the chaos theory intrigued and inspired many scientists and nourished their hope that it might finally prove conducive to an understanding and a numerical solution of the problem of turbulence. Irregular behaviour based on a few deterministic equations displays many characteristics also observed in turbulent flows, for example the sensitive dependence on small disturbances, the fundamental impossibility of long-term prognoses and the (statistically) self-similar structures as demonstrated by the

Phil. Trans. R. Soc. Lond. A (1993) **344**, 207–234
Printed in Great Britain

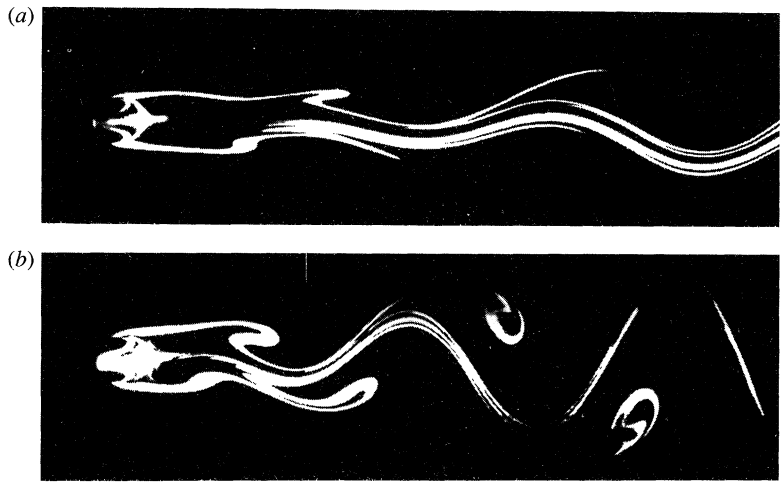

Figure 1. von Kàrmàn vortex street, stretching and folding (cf. Bergé *et al.* 1984).

hierarchies of eddies in a fully developed turbulence (Kolmogorov 1941). It proves helpful to classify the unsolved questions on turbulent flow under two headings, namely:

(*a*) the onset of turbulence; and

(*b*) the processes in a fully developed turbulence.

Promising and technically relevant answers have been established, at least in part, only for point (*a*).

Fully developed turbulent flows are not only characterised by temporally irregular behaviour but also by spatially disordered vorticial patterns on a broad spectrum of scales; both the temporal and spatial correlations extend, however, only over a short range. The less viscid the fluid under observation is, the smaller the smallest vortex becomes. Consequently, in a fully developed turbulence, a very large number of degrees of freedom (independent modes) must be considered (Grossmann 1990).

In the current chaos theory, however, it is tacitly assumed that the underlying phase space is of a relatively low dimension. In the following, we present a series of scenarios and mathematical models which lead to the development of chaotic, temporally irregular motions. On the other hand, spatial dependences in the underlying equations are not taken into account. Although the greater part of the questions on a fully turbulent flow thus remains unanswered, many of us believe that – particularly due to the universal character of some transitions – we can discern first signs which may lead in future to a deeper comprehension of complex processes such as turbulence.

Before we present the individual routes to chaos, we first refer to the fundamental phenomenon of mixing in turbulent motions. Figure 1 shows the development of a von Kàrmàn vortex street in the wake of a cylinder in an oncoming flow. The two photos clearly demonstrate the generation of the vortex pairs as a result of repeated stretching and folding of the flow lines. Interestingly, this is a mechanism we observe in the case of the Lorenz attractor when investigating the divergence of neighbouring trajectories. Although the actual stretching and folding does not take place in the physical space but in the phase space, the figure does impart an understanding of mixing and the sensitive dependence of the trajectories on small disturbances.

In 1976, the French astronomer and physicist, M. Hénon, considered two-

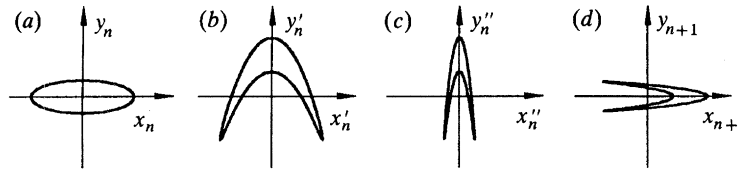

Figure 2. The three basic operations of the Hénon mapping of (1). The original domain (*a*) is (*b*) folded, (*c*) contracted and (*d*) mirrored.

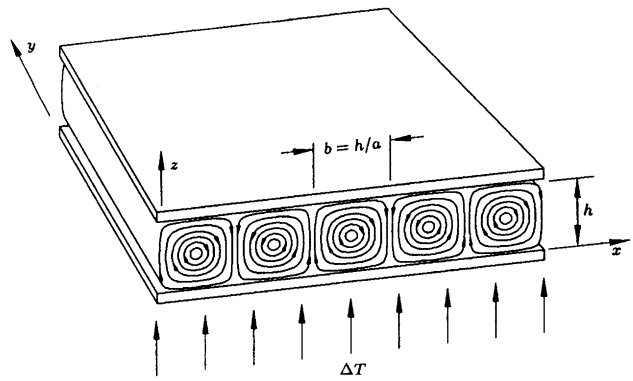

Figure 4. Rayleigh–Bénard experiment: layer of fluid between two plates subject to a temperature difference ΔT. An increase of ΔT leads to the transition from pure heat conduction to convection rolls.

dimensional recursion formulae in order to gain better insight into the microstructure of strange attractors (Hénon 1976). To this purpose, he analysed the mapping rule

$$x_{n+1} = 1 + y_n - \alpha x_n^2, \quad y_{n+1} = \beta x_n, \tag{1}$$

where each individual mapping step incorporates the three operations: folding, contracting and mirroring (figure 2). Continuous application of this sequence causes a total mixing of the initial points on the attractor (see figure 3, plate 1, for $\alpha = 1.4$, $\beta = 0.3$), a typical characteristic of turbulent flows and fundamental prerequisite for the unpredictability of the motion.

The discrete recursion formula (1) may be viewed as a Poincaré map of a continuous system and reproduces a long-term analysis of an evolutionary process, using sequential (stroboscopic) spot checks.

Let us illuminate the scene with a characteristic illustration of phenomena occurring in purely temporal processes. At the beginning of the 1960s, the meteorologist Edward N. Lorenz developed a highly simplified weather model (Lorenz 1963) on the basis of the Rayleigh–Bénard experiment (figure 4). This model demonstrated that even only three ordinary nonlinear differential equations can cause aperiodic chaotic behaviour and that thus, long-term weather forecasts are impossible on principle. To solve the set of partial differential equations describing the convective flow, Lorenz developed the temperature and velocity fields in Fourier series, taking only three modes, one stable and two unstable, into account. This led to the aforementioned system of three ordinary, nonlinear coupled differential equations, the Lorenz system

$$\dot{X} = -\sigma X + \sigma Y, \quad \dot{Y} = rX - Y - XZ, \quad \dot{Z} = -bZ + XY. \tag{2}$$

Here, the X-mode describes the flow field, Y and Z define changes in the horizontal

and vertical directions of the temperature field, σ is the Prandtl number, b characterizes the geometry of the convection rolls and r is the relative Rayleigh number which is proportional to the applied temperature difference ΔT. Lorenz realized that for $\sigma = 10$, $r = 28$, $b = 8/3$ the slightest deviations in the initial conditions lead to great differences in the long-term behaviour. Then, trajectories which are originally neighbouring deviate from each other exponentially. Nevertheless, for all the disorderliness of the trajectories, these form in the long-term a strange attractor within a limited domain of the phase space, the Lorenz attractor. Lorenz's model may have been criticized justly for not providing a perfect model for the Bénard-convection problem. However, it illustrates with remarkable intensity the development of chaotic solutions in nonlinear differential equations.

Figure 5, plate 2, illustrates some characteristics of the strange attractor using the Lorenz attractor as an example. Figure 5*a*, *b* demonstrates irregular behaviour: the trajectory jumps in a stochastic, unpredictable way from one branch of the attractor to the other; each jump is portrayed graphically by a change of colour. Figure 5*c* shows the characteristic of attraction on the basis of two different initial conditions: following a transient phase, all the orbits are attracted to a bounded domain of the phase space. Figure 5*d* illustrates the sensitive dependence on the initial conditions: two orbits, one red and one blue, with initial conditions deviating only minimally from one another, diverge exponentially after some time. These illustrations show that in spite of locally chaotic behaviour, there are coherences in the phase space which generate a global geometrical structure, an expression of the underlying deterministic laws.

Figure 6, plate 2, again demonstrates impressively the divergence of neighbouring trajectories causing ultimately a mixing and spreading over the attractor. In fact, 15000 initial conditions are chosen on one minute line segment and the associated trajectories calculated and recorded stroboscopically. At first, the line segment stretches to a long line, which is elongated repeatedly, folded back and finally spread out as a cloud over the whole attractor. Each measurement, however precise it may be, contains small errors. Chaotic systems magnify these microscopic fluctuations exponentially to such an extent that after a finite period of time, they become visible on a macroscopic scale.

We now reconsider the solution of the Lorenz equation (2) and offer a computer generated evolution of the solution as a function of the relative Rayleigh parameter r.

Because of the complexity of phenomena in the phase space we begin with a short overview. In particular, we present in figure 7 the development of various attractor and bifurcation types for the parametric values $\sigma = 10$ and $b = 8/3$ (Sparrow 1982; Guckenheimer & Holmes 1983).

For $0 < r < 1$, we recognize only one single fixed point placed at the origin. The eigenvalues of the linearized flow at this fixed point are

$$\lambda_{1,2} = -\tfrac{1}{2}(\sigma+1) \pm \tfrac{1}{2}\sqrt{[(\sigma+1)^2 + 4(r-1)\,\sigma]}, \quad \lambda_3 = -b. \tag{3}$$

All three eigenvalues in this r-range possess negative real parts, the origin is thus a stable node. For increasing r, the real part of one eigenvalue becomes zero for $r = 1$; the others remain negative. We observe a classic example of a pitchfork bifurcation. The newly developing states of equilibrium C_2, C_1 for $r > 1$ possess the coordinates $\{\pm\sqrt{[b(r-1)]}, \pm\sqrt{[b(r-1)]}, (r-1)\}$ in the phase space. The characteristic equation for their eigenvalues in the linearized system is

$$\lambda^3 + \lambda^2(\sigma+b+1) + \lambda(\sigma+r)\,b + 2\sigma b(r-1) = 0. \tag{4}$$

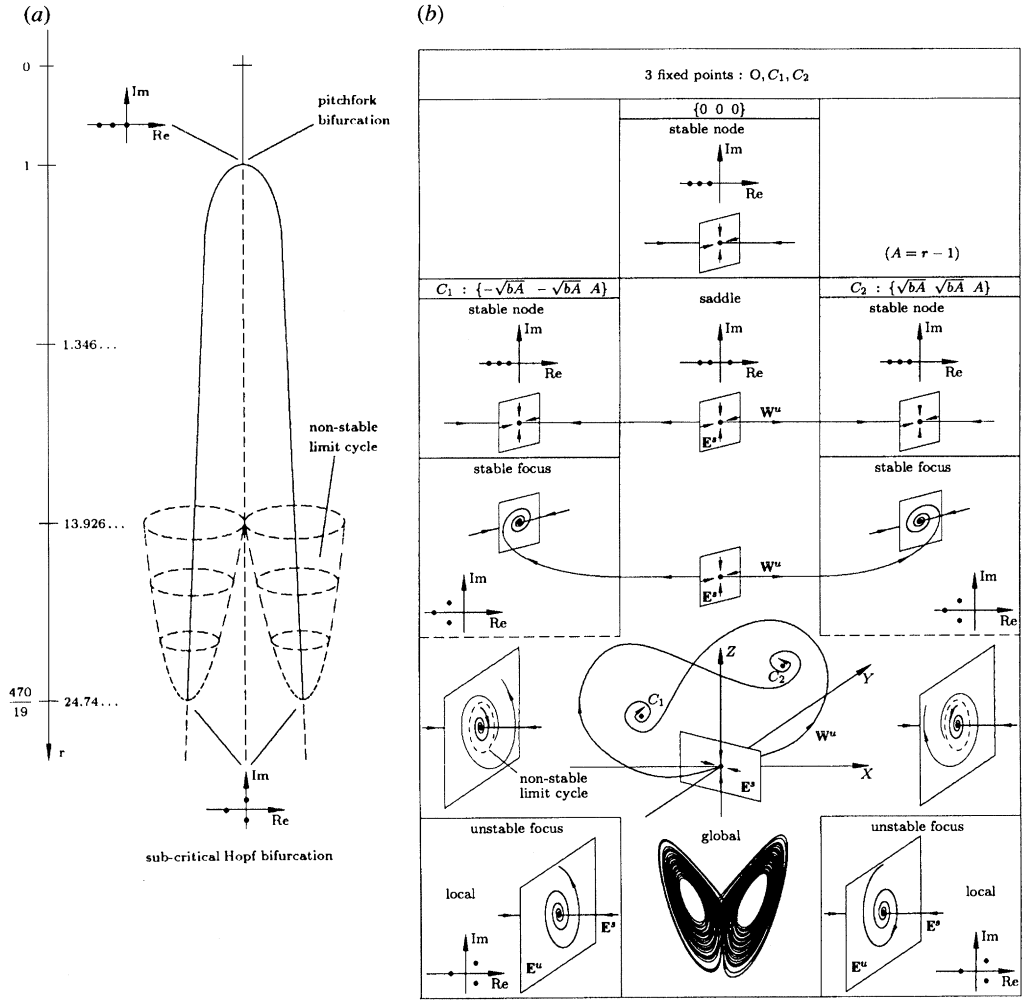

Figure 7. Lorenz system for $\sigma = 10$, $b = 8/3$ and a variable r. (*a*) Bifurcation diagram. (*b*) Evolution of fixed points.

All three eigenvalues are real and negative for $r < 1.346\ldots$, i.e. the fixed points C_1, C_2 are stable nodes. For $r = 1.346\ldots$, two eigenvalues coalesce and emerge for increasing r as pairwise conjugate complex values. The attractor type is transformed from a stable node to a stable focus. As the pitchfork bifurcation evolves the origin is seen to become at $r = 1$ unstable in one direction and retains its saddle node character for all $r > 1$.

We now concentrate on the flow in the range $1.346\ldots < r < 13.926\ldots$. The eigenvalue constellation at the origin – $\mathrm{Re}\,(\lambda_1)$, $\mathrm{Re}\,(\lambda_2) < 0$ and $\mathrm{Re}\,(\lambda_3) > 0$ – conditions a two-dimensional stable and a one-dimensional unstable manifold (see figure 8, plate 3). If we trace the unstable manifold of the origin numerically, we observe that the associated flow is captured by the two foci C_1 and C_2. The question is: how does the two-dimensional stable manifold at the origin evolve respectively where do the trajectories that form the stable manifold of the origin come from. The upper four illustrations of figure 8, plate 4, demonstrate the development of the stable manifold. To analyse it numerically we reverse the time-history of the

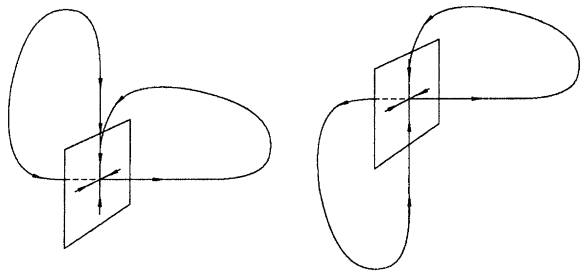

Figure 11. Two homoclinic orbits at the origin (Wiggins 1988).

trajectories which shape this surface by proceeding in a negative t-direction. In this case, the trajectories describe a surface that can be viewed in a good approximation as the exact one. To pursue the twistings of the surfaces in the phase space more clearly, the front of the surface is coloured red and the back blue.

The coloured illustrations of figure 8 show that the stable manifold spreads between the two unstable branches around the positive Z-axis and then twists itself around the two loops generated by the two foci. As the surface embraces the loops around C_1 and C_2, it returns to the origin, with one difference, that the red front becomes the reverse side, and the blue back takes the place of the front. Since trajectories in the phase space cannot intersect for reasons of uniqueness (Cauchy), the blue surface following its return to the origin can only continue to its progress by a downward folding action. If we follow the flow emanating from a number of initial points either on the blue or on the red side, we obtain the required information on the respective basins of attraction of C_1 and C_2: trajectories with initial points in the blue domain always end in the left focus, initial points in the red domain in the right focus. The spiral loops of the unstable manifolds which unwind in very close twists around C_1 and C_2 for r-values just above 1 are seen to expand continuously with increasing r. At the parameter value $r = 13.926\ldots$, we observe that the respective branches of the unstable manifold return to the origin as stable manifolds. In this case, when the trajectory progresses to the same point for $t \to -\infty$ and $t \to +\infty$, we speak of a homoclinic orbit. Figure 11 shows two homoclinic orbits at the origin. A further increase of r – the real parts of the eigenvalues display no zero passage – causes a surprising escaping action of the trajectories emanating from the right to the left fixed point and of those emanating from the left to the right fixed point (see figure 9, plate 4). This significant alteration of the orbital structure due to the parameter alteration in r is a typical example of a global bifurcation (Wiggins 1988).

We next inquire into the paths the trajectories forming the stable manifold at the origin adopt in this new, highly complex situation. The first four illustrations of figure 9 demonstrate this development for $r = 15 > 13.926\ldots$. The surface unfolds as in figure 8 with one difference: the surface on its return to the origin is unable to fold downwards since this passage is barred by the unstable trajectories. The rule of figure 8 that all initial points on the red hemisphere move to the right focus and all blue ones to the left focus is now no longer true for all initial conditions.

An increase of r to $r = 470/19 = 24.74\ldots$, leads to the sub-critical Hopf bifurcation shown in figure 7. The fact that a strange attractor, the Lorenz attractor, is formed around and in association with the unstable fixed points C_1 and C_2 for $r > 24.74\ldots$, is the really surprising result of the Lorenz system.

Having discussed some typical characteristics of the Lorenz attractor we attempt

here to elucidate the geometry of this exotic structure which represents a hybrid form between a surface and a spatial object (see figure 10, plate 4). We remember that in the chaotic domain (figure 5), the left and the right branches of the unstable manifold of the origin spiral unstably around C_1 and C_2 and jump unpredictably and without warning from left to right and back again. The stable two-dimensional manifold at the origin now has to wind its way through this chaotic intricacy of lines. The mille-feuille-like structure can be clearly recognized in the phase space. We know that the mille feuille layers lie infinitely close to one another; this means that a division into blue and red spatial realms becomes practically impossible. In this sea of uncertainty an initial point cannot decide if its allegiance belongs to the red or blue fractions. This local indecisiveness of the stable manifold within the realm of a strange attractor is a further – here narrated in a more geometrical context – characteristic of a local unpredictability of this type of attractor.

The great British scientist Osborne Reynolds realized as long as a hundred years ago that the Navier–Stokes equations contain only one essential control parameter, namely the Reynolds number Re, which determines the character of the fluid flow. In the case of a small Re, the flow is laminar; if the Re is increased, turbulent behaviour sets in from a critical Reynolds number onwards at least so intermittently. Indeed, nowadays we suspect that the standard Navier–Stokes equations, as Heisenberg first conjectured, do not include all ingredients to interpret all aspects of turbulence.

One of the important tasks of the theory of dynamical systems is to establish ordering principles for the multitude of transitions from stationary to chaotic behaviour when one or more control parameters are varied; further, to construe theoretical models of instability hierarchies which explain the individual routes to chaos qualitatively and can be verified quantitatively by experiment. It is easy to comprehend the complexity of this task if one recollects that even for a single control parameter the local bifurcations of states of equilibrium alone can be divided into four categories having different normal forms and different characteristics of symmetry. Hence, it is obvious that there cannot only be one single scenario describing the transition from regular to chaotic behaviour, but that a series of alternative mathematical models have to be considered. Which route a particular system will follow is not yet evident on the basis of present findings, but it certainly depends on inherent symmetries and conservation rules in the physical domain of the system.

We continue our description on the onset of turbulence with a short survey of instability hierarchies appertaining to local bifurcations as proposed by a number of scientists.

Limitation of space precludes the exploration of other important transitions to chaos arising through global bifurcations. An increase of the controlling system parameter may also generate a qualitative change in the topological characteristics of the invariant manifolds leading to a radically different response. The Lorenz system is a representative model displaying the significance of global inquiries necessary for a comprehension of the cause of chaotic behaviour. In this example the sub-critical Hopf bifurcation at $r = 24.74$ (see figure 7) is almost irrelevant to the formation of the strange attractor. There is rather a variety of striking global changes, specifically homoclinic and heteroclinic bifurcations, in the parameter range of $1 < r < 24.74$ between the local bifurcations of fixed points leading to chaotic dynamics (for details see Sparrow 1982; Guckenheimer & Holmes 1983). (We

PHILOSOPHICAL TRANSACTIONS OF THE ROYAL SOCIETY A MATHEMATICAL, PHYSICAL & ENGINEERING SCIENCES

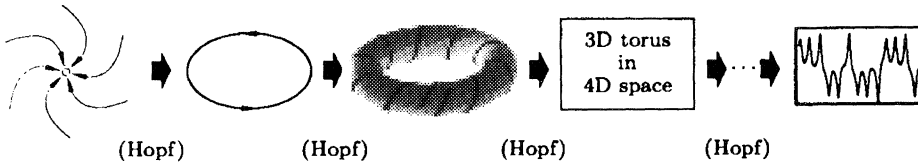

Figure 12. Landau's turbulence model.

gratefully acknowledge the comment of a referee stressing the significance of the role global bifurcations play for the onset of chaos.)

2. Routes to chaos

We now survey some pertinent routes to chaos.

(*a*) *Landau's route to chaos*

One of the first mathematical models that offered a description of the transition from laminar to turbulent flow was developed by the distinguished Russian physicist Lev Landau (1944). He assumed that a steady increase of the Reynolds number which plays the role of a free control parameter μ leads to an infinite sequence of instabilities: if the initial stationary state which corresponds to a fixed point in the phase space becomes unstable, then a Hopf bifurcation (Hopf 1942) occurs resulting in a limit cycle, i.e. a periodic motion with a frequency f_1. Following a further increase of μ, the limit cycle also becomes unstable and undergoes a bifurcation into a two-dimensional torus; this entails the emergence of a second incommensurable frequency f_2 and a quasi-periodic motion. Landau now assumed that a further increase in the control parameter leads to a series of generalized Hopf bifurcations with a continuously increasing number of incommensurable frequencies (figure 12) and that turbulent behaviour ultimately consists of complex quasi-periodic motions on an ∞-dimensional torus.

The deficiencies of Landau's turbulence model did not emerge until the 1970s when the chaos theory was conceived. Quasi-periodic motions on a torus do not in fact react sensitively to small disturbances in the initial conditions and do not entail mixing in the phase space, two characteristic features of turbulent flow.

(*b*) *Ruelle–Takens scenario*

Without being aware of Edward Lorenz's work, which had appeared in a special meteorological journal, Ruelle & Takens (1971) conceived a completely different scenario. The theory does not content itself with finding solutions as the Landau scenario does but explores also with the support of qualitative dynamics the nature of solutions, in particular, if they are stable and in addition generic. The concept 'generic' is often used in mathematics nowadays and refers to *typical* characteristics that are the rule and not the exception. Ruelle & Takens proved that Landau's idea of a transition to turbulence after a cascade of so many Hopf bifurcations was highly untypical and that even a motion on a three-dimensional torus becomes unstable in the generic case. They showed that typically, a *strange attractor* emerged immediately after the third bifurcation. This strange attractor does, however, have a different evolution history to that of the Lorenz attractor shown in figure 7. In contrast to Landau's scenario, only a small number of degrees of freedom are sufficient to describe chaotic behaviour. Figure 13 presents the Ruelle–Takens scenario.

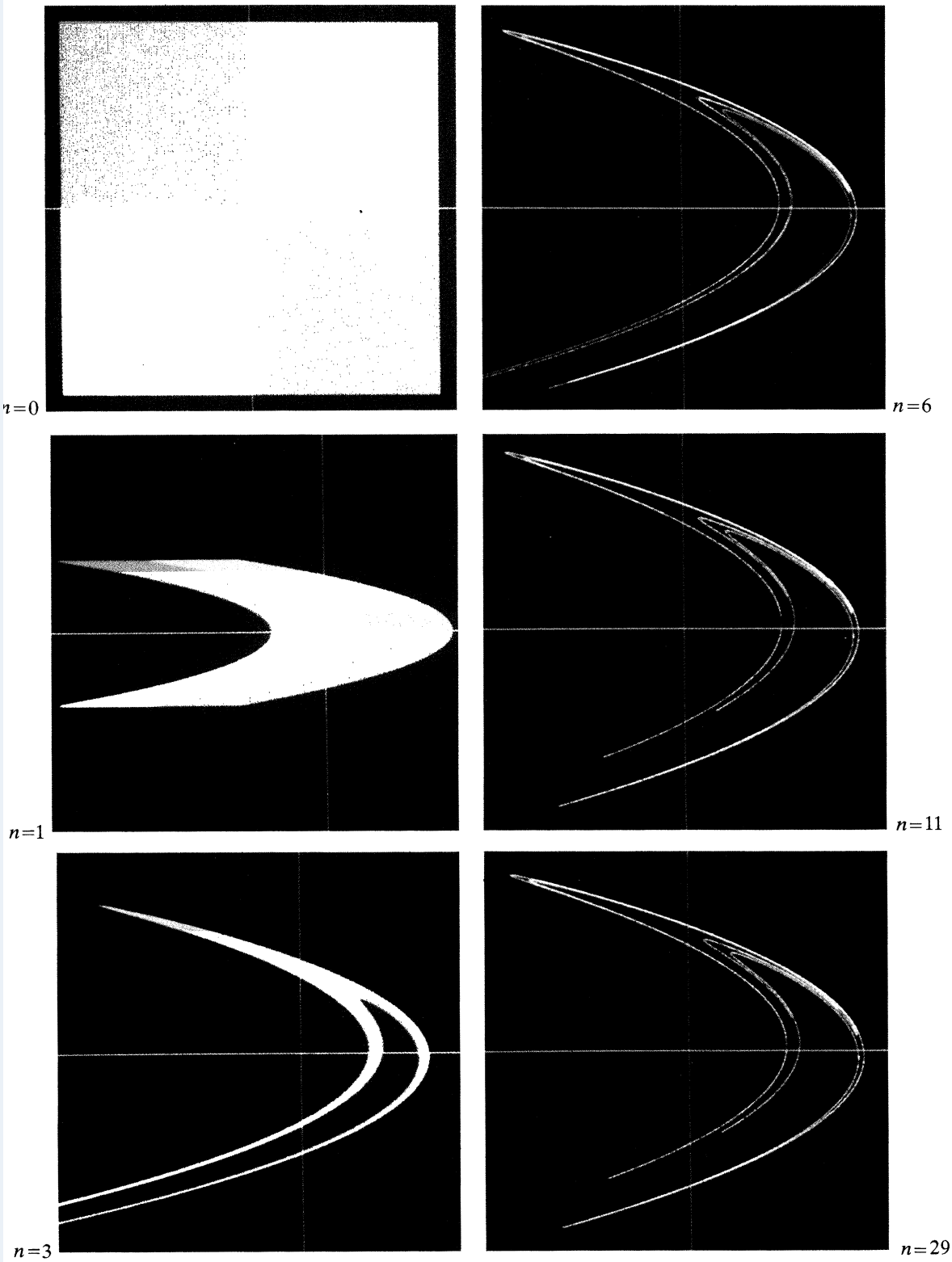

Figure 3. Formation of the Hénon attractor: initial conditions ($n = 0$) assigned to four coloured areas; complete mixing after $n = 29$ iterations.

PHILOSOPHICAL TRANSACTIONS OF THE ROYAL SOCIETY A MATHEMATICAL, PHYSICAL & ENGINEERING SCIENCES

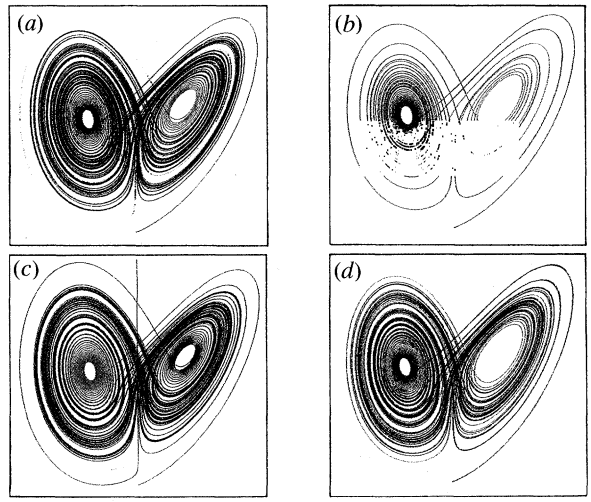

Figure 5. Lorenz attractor for $r = 28$, $\sigma = 10$, $b = 8/3$. (*a*), (*b*) Unpredictable jumps, (*c*) basin of attraction, (*d*) sensitive dependence upon initial conditions.

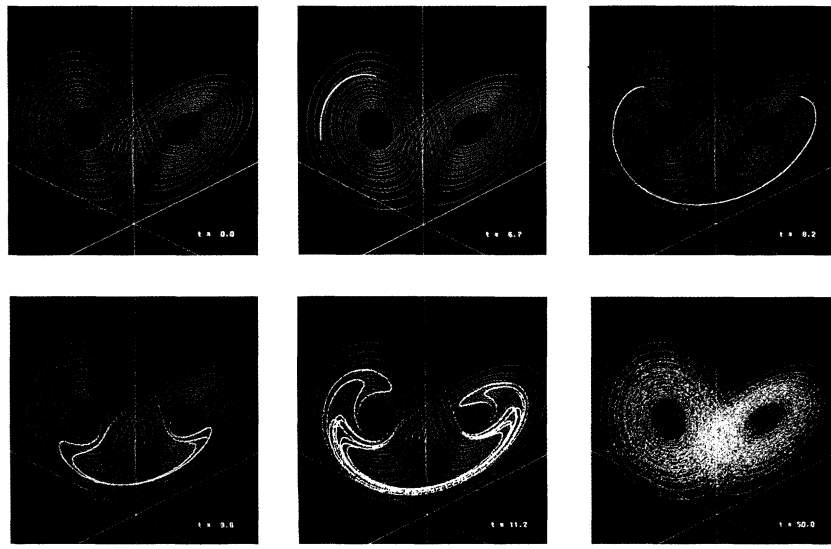

Figure 6. Divergence of neighbouring trajectories.

PHILOSOPHICAL TRANSACTIONS OF THE ROYAL SOCIETY A MATHEMATICAL, PHYSICAL & ENGINEERING SCIENCES

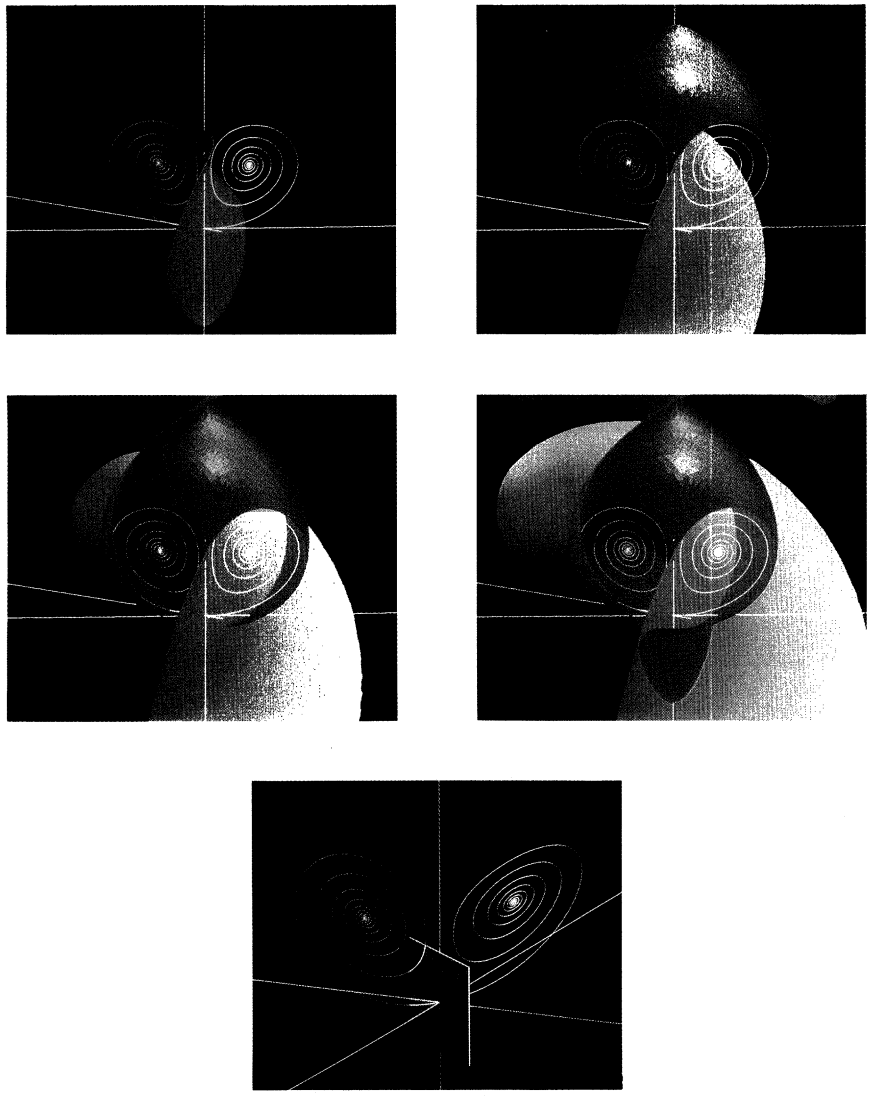

Figure 8. Evolution of the stable manifold (surface) and the unstable manifold (line) appertaining to a fixed point in the origin ($r = 12$).

PHILOSOPHICAL TRANSACTIONS OF THE ROYAL SOCIETY A MATHEMATICAL, PHYSICAL & ENGINEERING SCIENCES

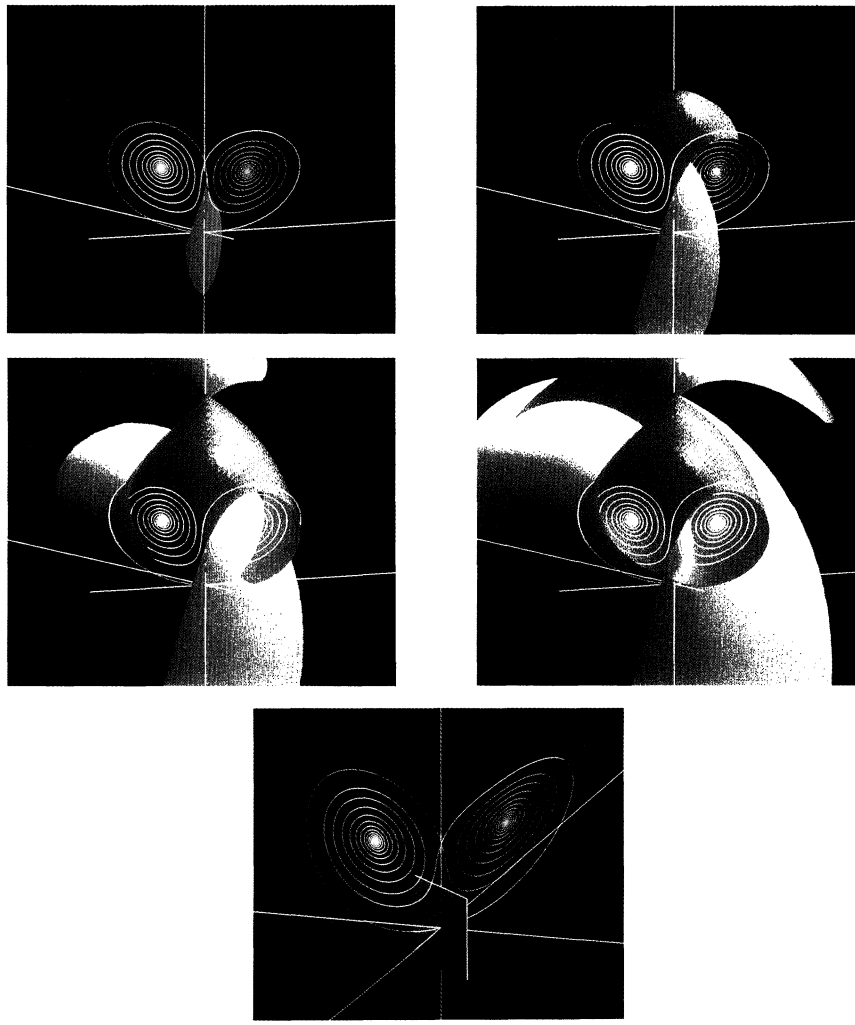

Figure 9. Evolution of the stable manifold (surface) and the unstable manifold (line) appertaining to a fixed point in the origin ($r = 15$).

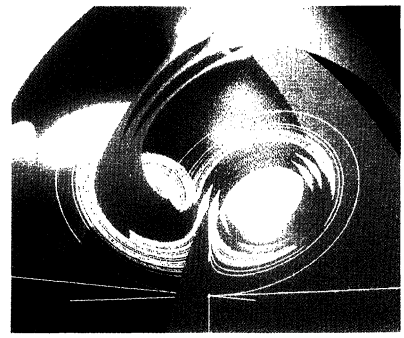

Figure 10. Lorenz attractor ($r = 28$).

PHILOSOPHICAL TRANSACTIONS OF THE ROYAL SOCIETY A MATHEMATICAL, PHYSICAL & ENGINEERING SCIENCES

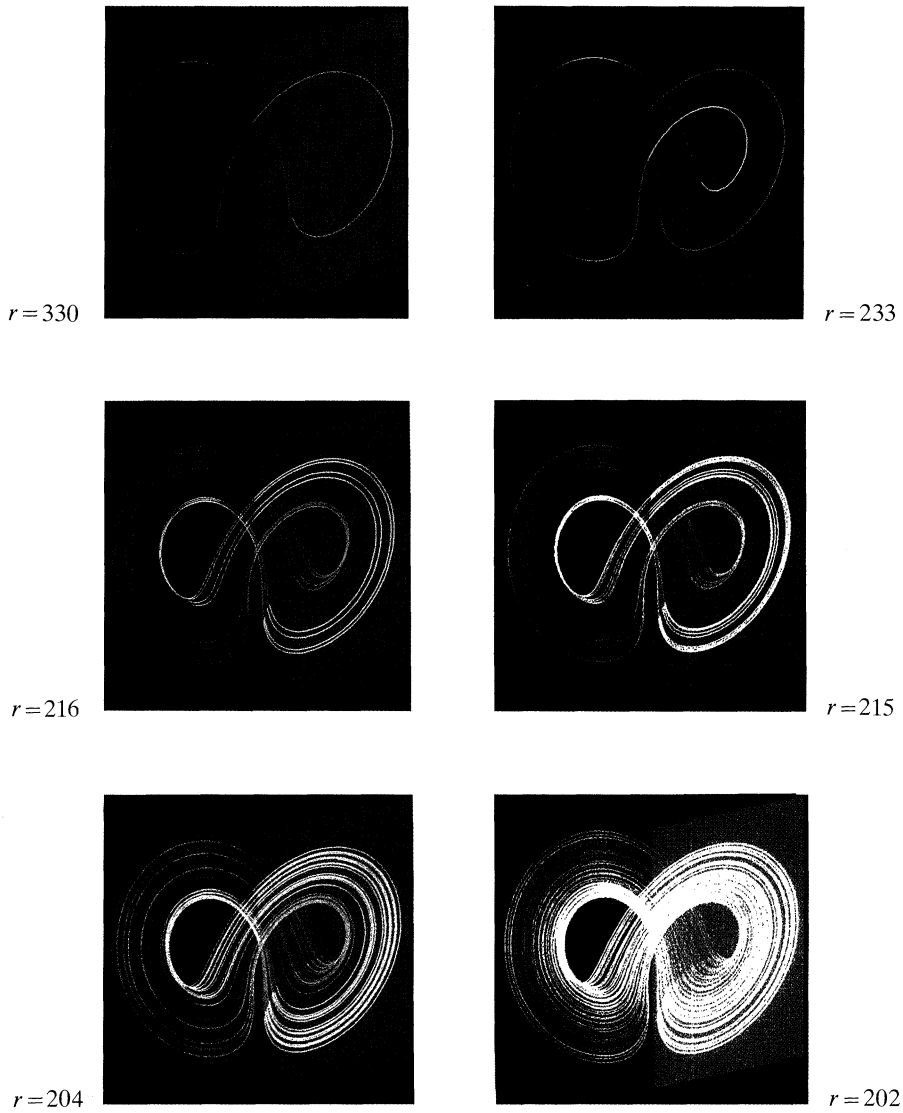

Figure 22. Lorenz system: co-existence of two attractors and inverse cascade of period doublings.

PHILOSOPHICAL TRANSACTIONS OF THE ROYAL SOCIETY A MATHEMATICAL, PHYSICAL & ENGINEERING SCIENCES

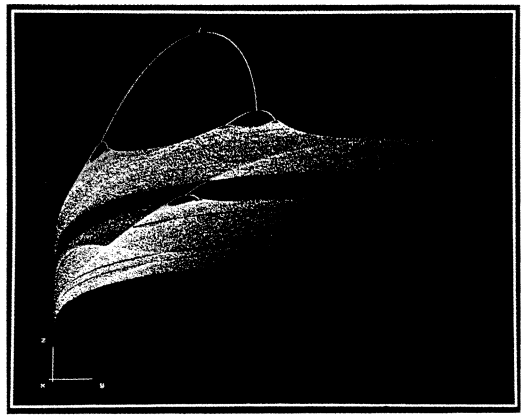

Figure 23. Bifurcation diagram of the Poincaré sections of the Lorenz system for $25 \leqslant r \leqslant 325$.

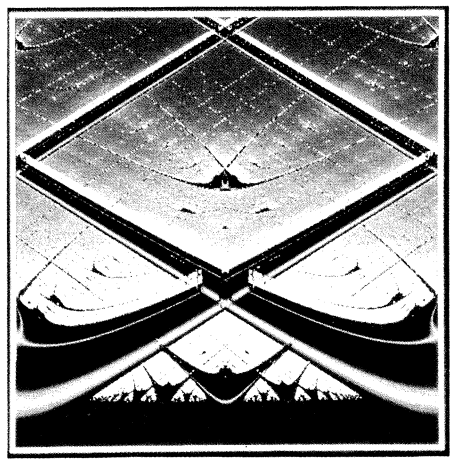

Figure 26. Lyapunov exponent $\sigma(\Omega, K)$ for the circle mapping $(0 \leqslant \Omega \leqslant 1, 0 \leqslant K \leqslant 10)$.

PHILOSOPHICAL TRANSACTIONS OF THE ROYAL SOCIETY A MATHEMATICAL, PHYSICAL & ENGINEERING SCIENCES

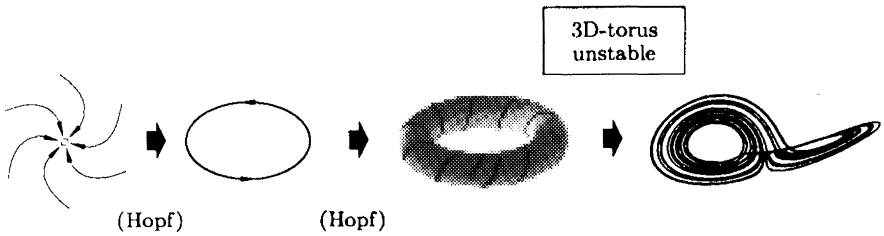

Figure 13. Ruelle–Takens scenario.

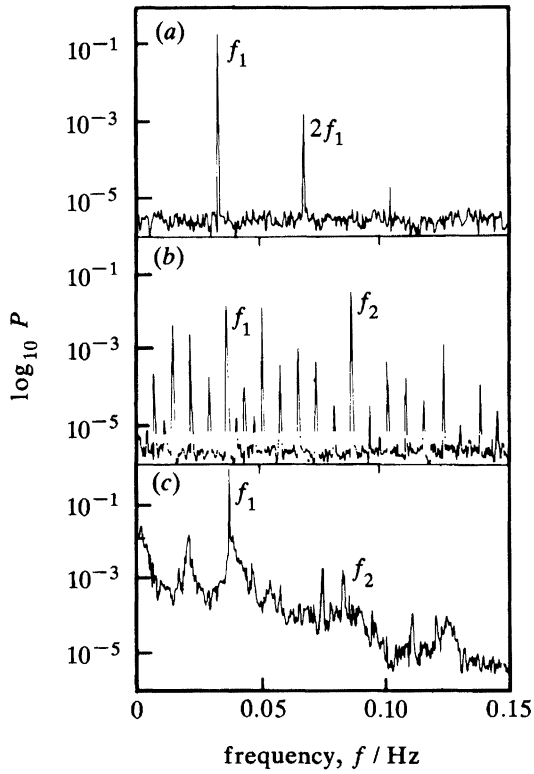

Figure 14. Experiment of Swinney & Gollub (1978): power spectra for the Rayleigh–Bénard convection.

It proved possible to confirm Ruelle & Takens' theory experimentally by means of highly sensitive measuring devices such as the laser-Doppler technique. For this purpose, flow experiments had to be conceived where the boundary conditions impose a freezing of the spatial structure, thus activating only a small number of spatial modes and conditioning an onset of turbulence due to purely temporal processes.

The first experiment allowing a sufficiently precise observation of the transition to turbulent behaviour according to Ruelle–Takens was carried out by Gollub & Swinney (1975) for the Taylor–Couette flow and for the Rayleigh–Bénard convection (Swinney & Gollub 1978). Application of the power spectral method for increasing relative Rayleigh numbers R, recorded in figure 14, shows (*a*) a periodic oscillation of the convection rolls with a fundamental frequency f_1, (*b*) a quasi-periodic motion with two incommensurable fundamental frequencies f_1 and f_2 (the power spectrum

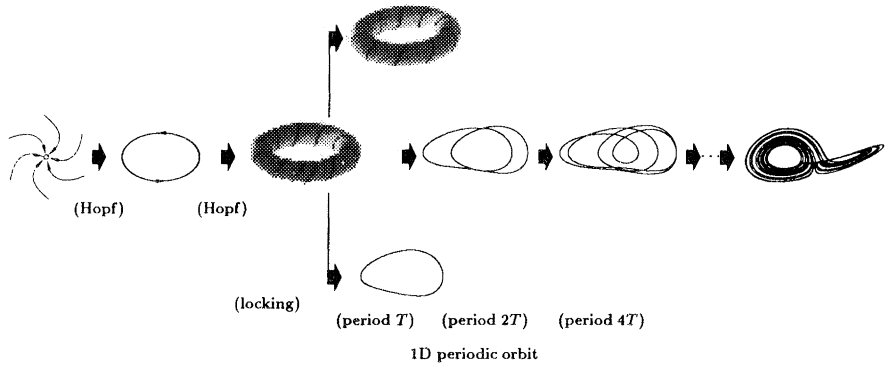

Figure 15. Feigenbaum's scenario: via period doublings to chaos.

shows sharp peaks for f_1 and f_2 and their linear combinations) and (*c*) a broad band spectrum with some sharp peaks which indicate the emergence of a chaotic motion. A first interpretation of the power spectra may make us believe, of course, that very many active modes are generating the irregular motion. Application of the Packard and Taken's reconstruction technique (Packard *et al.* 1980; Takens 1981) shows, however, a strange attractor of the correlation dimension $D_C \approx 2.8$ (Hentschel & Procaccia 1983). This could be deduced from the time history response (Malraison *et al.* 1983) and confirms that the transition is identical with Ruelle and Takens' scenario. Immediately after the third Hopf bifurcation, chaos sets in.

(*c*) *The period doubling cascade: Feigenbaum's route to chaos*

In many experiments, it can be observed that an increase in the system parameter μ beyond the second generalized Hopf bifurcation on the two-dimensional torus is followed by a synchronization (locking) of the two incommensurable frequencies so that the quasi-periodic behaviour is succeeded by a periodic motion. The limit cycle which thus emerges also becomes in its turn unstable following an increase of μ and undergoes a flip bifurcation which results in period doubling. The new limit cycle then goes through a cascade of period doublings until chaos sets in (see the schematic illustration in figure 15). In his work at the end of the 1970s, the American physicist M. Feigenbaum (1979*a*) succeeded in discovering the universal character of this transition by establishing a link with more general second-order phase transitions. Such a continuous phase transition is displayed by ferromagnets, for example, which lose their permanent magnetization above a critical temperature, the so-called Curie temperature. At the end of the 1960s and beginning of the 1970s, Kenneth Wilson (1971) succeeded in developing an explicit formulation of the renormalization group theory which made possible a quantitative determination of the critical exponents which define the phase transition; this led to a classification of a whole series of second-order phase transitions in categories of universality (for an introductory work see Lipowsky 1983). Inspired by the renormalization group theory, Feigenbaum studied the transition to chaos in a very simple nonlinear mapping rule which had already been used to describe biological populations (May 1976)

$$x \to f(x) = \alpha x(1-x). \tag{5}$$

For $0 < \alpha < 4$, the unit interval $I = [0, 1]$ is mapped into itself. In spite of the simple set-up of this iteration rule $x_{n+1} = f(x_n)$, the long-term behaviour of the sequence $\{x_n\}$ varies for $n \to \infty$ dramatically in dependence on the control parameter α.

The fixed points of the map are $x = 0$ and $x = 1 - 1/\alpha$. For $0 < \alpha < 1$, it suffices to consider only the stable fixed point $x = 0$ in this α-range. The stability of this fixed point is reversed for $\alpha = 1$ and the point becomes unstable. A transcritical bifurcation takes place; the formerly unstable fixed point $x = 1 - 1/\alpha$ becomes stable and advances into the unit interval I (figure 16*a*). Following a further increase of α, this state of equilibrium also loses its stability; for $\alpha_1 = 3$, a flip bifurcation takes place and a 2-cycle emerges, i.e. a periodic motion (figure 16*b*). Increasing α up to a 2nd critical value $\alpha = \alpha_2$, the motion becomes once more unstable and a period doubling occurs (figure 16*c*).

Further incrementation of α leads to a whole cascade of period doublings until finally, when a critical value α_∞ is attained, chaotic behaviour sets in (figure 16*d*).

In figure 17*a*, we present the bifurcation diagram, i.e. the long-term behaviour in dependence of α for the logistic mapping, and underneath, in figure 17*b*, the corresponding Lyapunov exponent σ which is a measure of the stability of the motion. At the critical points α_k where period doublings occur, σ vanishes as to be expected. Between two sequential critical values α_k and α_{k+1} lies a value A_k for which the motion on a cycle of the period 2^k is superstable, i.e. $(f^{2^k})' = 0$ applies at all cycle points. At these points, the theoretical value of the Lyapunov exponent is $\sigma = -\infty$; numerically, a large but finite negative value is obtained. For $\alpha > \alpha_\infty$, chaotic motion sets in, reflected in positive values of σ. This irregular behaviour is continuously interrupted by periodic windows, i.e. by α-ranges in which cycles of the period m ($m \in \mathbb{N}$) occur and which in turn again progress into chaos via period doubling cascades.

The bifurcation diagram is self-similar with regard to both the variable x and the control parameter α: each new branch reproduces the whole course on a smaller scale. This behaviour is denoted as a self-similarity. Feigenbaum's numerical studies (1979*a*) showed the following.

1. The distances between successive bifurcation points satisfy a rule of a geometrical progression

$$\lim_{k\to\infty} \frac{\alpha_{k+1} - \alpha_k}{\alpha_{k+2} - \alpha_{k+1}} = \delta. \tag{6}$$

2. The distance d_k of the specific point in the superstable 2^k-cycle which lies nearest to $x = \frac{1}{2}$ (figure 17*a*) also decreases geometrically. Noting the standard directional convention for the sign of the distance d_k we have

$$\lim_{k\to\infty} \frac{d_k}{d_{k+1}} = -a. \tag{7}$$

Applying the *renormalization technique*, Feigenbaum succeeded in decoding the self-similar structure of the bifurcation diagram, i.e. in determining the values of a and δ theoretically. It is possible to comprehend the mechanism of period doubling if one observes a 2^k-fold iterate ($k = 1, 2, \ldots$) of the initial function $f(x)$. Feigenbaum introduced an iteration operator T^* which, if applied on a function $f(x)$, e.g. the logistic expression, generates an iteration step involving a shift of the system parameter α and a simultaneous scaling. In this way we obtain for $k \gg 1$

$$T^* f_{A_k}(x) \sim -a f^2_{A_{k+1}}(-x/a). \tag{8}$$

Here, the index A_k represents the current value of α in (5). The interpretation of the operator T^* is shown schematically in figure 18. An n-fold application of the operator T^* to the series of functions $f_{A_1}, f_{A_2} \ldots$, generates for $n \to \infty$ a series of limiting

PHILOSOPHICAL TRANSACTIONS OF THE ROYAL SOCIETY A MATHEMATICAL, PHYSICAL & ENGINEERING SCIENCES

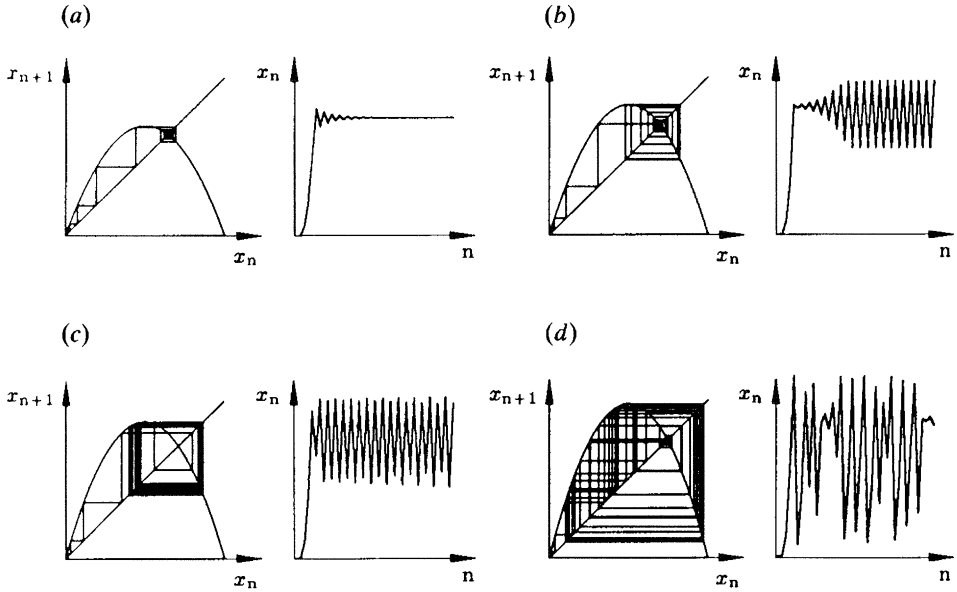

Figure 16. Iteration of the logistic mapping $x_{n+1} = \alpha x_n(1-x_n)$: (*a*) $\alpha = 2.8$, fixed point; (*b*) $\alpha = 3.3$, periodic motion; (*c*) $\alpha = 3.48$, period doubling; (*d*) $\alpha = 3.9$, chaos.

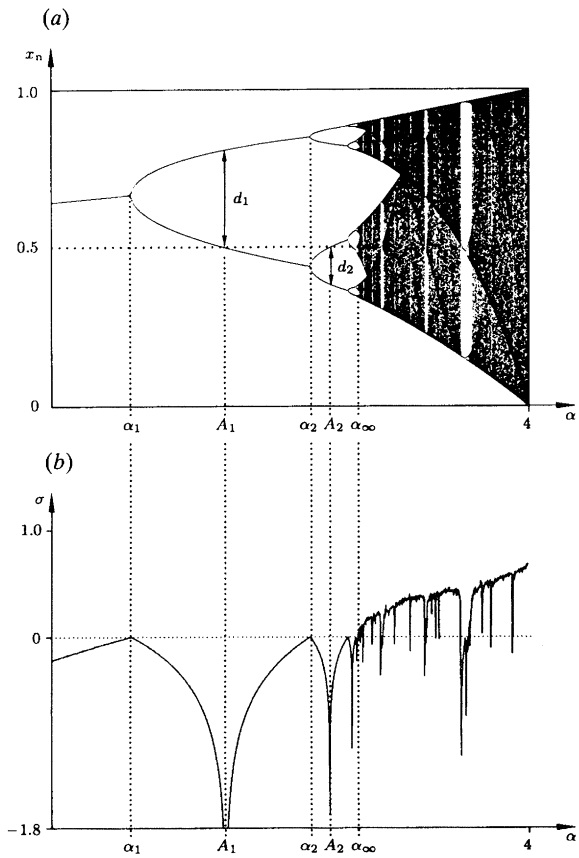

Figure 17. Bifurcation diagram and Lyapunov exponent for the logistic mapping.

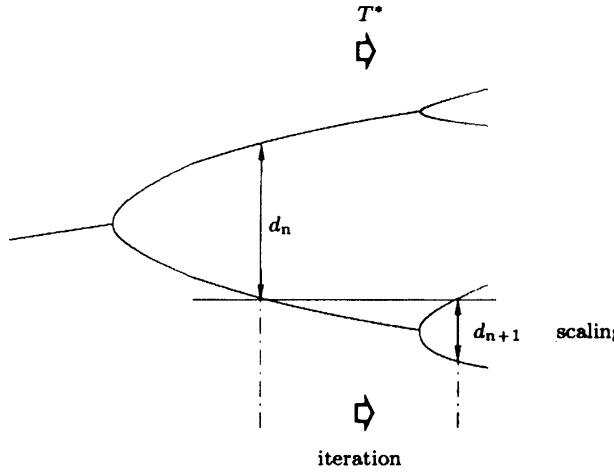

Figure 18. Schematic representation of the operator T^*.

functions $g_1, g_2 \ldots$. The crucial point here is that for each $i = 1, 2 \ldots$, the rescaled iterates $f^{2^n}_{A_{n+i}}$ converge for $n \to \infty$ in the neighbourhood of the central extremum to a function $g_i(x)$. These limiting functions fulfil via a doubling transformation T the condition

$$g_{i-1}(x) = Tg_i(x) = -ag_i(g_i(-x/a)). \tag{9}$$

In fact, T operates on a function space and leads within this space to a 'fixed point' $g(x)$, i.e. a universal function which reproduces itself following a doubling transformation

$$g(x) = Tg(x) = -ag(g(-x/a)). \tag{10}$$

This characterizes a transition to chaos. A specification of the maximum of f and hence g yields by application of (10) the Feigenbaum constant a as well as the Taylor approximation of $g(x)$. As in the linear stability analysis, it is also possible here to specify the nature of the stability of this 'fixed point'; in the present case, however, functions take on the role of points in the phase space and the operator T the role of a functional instruction. It transpires that $g(x)$ corresponds to a saddle-point and the Feigenbaum constant δ defines the positive eigenvalue of the linearized operator T at the point $g(x)$ in the direction of the unstable manifold $\mathbb{W}^u$.

At this stage we should be reminded that the calculations depend only on the nature of the maximum of the mapping function $f(x)$ and not on the details of its functional variation. In particular, for quadratic maxima as is the case for the logistic map, the two Feigenbaum constants are given by

$$a = 2.502\,907\,87 \ldots \tag{11}$$

and

$$\delta = 4.669\,201\,66 \ldots. \tag{12}$$

These constants possess universal character in the sense that their values do not derive from the details of the underlying dynamical system but only from the order of the maximum of its Poincaré mapping. Period doubling transitions could indeed be observed and quantitatively confirmed in such differing systems as electrical circuits (van Buskirk & Jeffries 1985), population dynamics (May 1976) and convective flows.

In 1978, Libchaber & Maurer began a series of experiments investigating the generation of turbulence in Rayleigh–Bénard cells of liquid helium. The ingenious way they set up their experiment and the highly sensitive measuring devices used

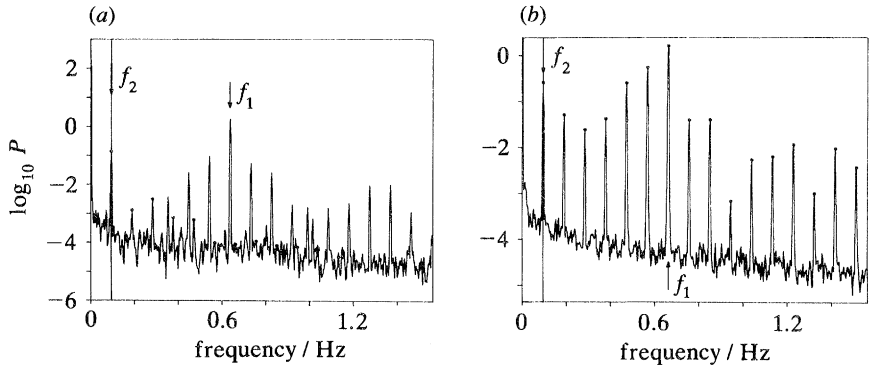

Figure 19. Frequency locking in the Rayleigh–Bénard experiment (Maurer & Libchaber 1979). (*a*) $R = 2.98 \times 10^4$, (*b*) $R = 3.3 \times 10^4$.

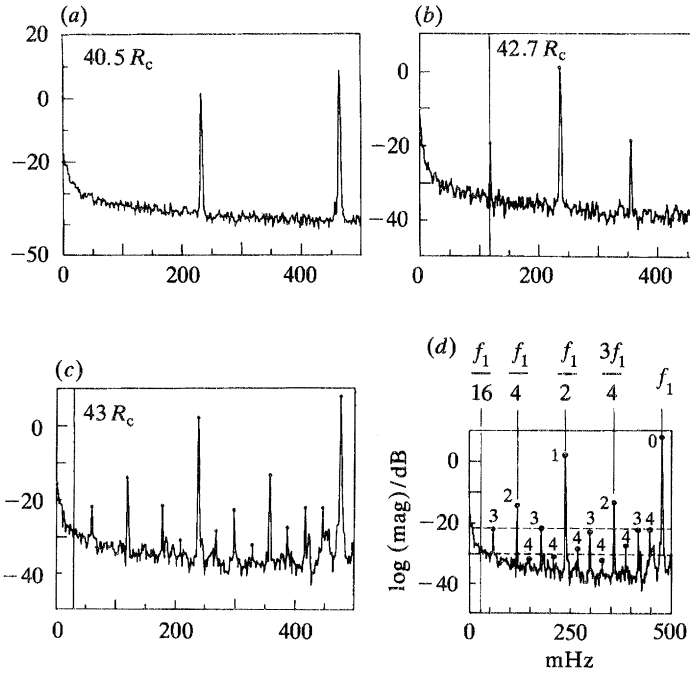

Figure 20. Bénard convection: period doubling cascade (*a*)–(*c*) and scaling laws (*d*) emerging in the power spectrum (Libchaber & Mauer 1980; cf. Schuster 1988). (*a*) $40.5R_c$, (*b*) $42.7R_c$, (*c*), (*d*) $43R_c$.

enabled them to achieve extremely precise measurements. Figure 19 shows the power spectra appertaining to two Rayleigh numbers taken from their work. The line spectrum in figure 19*a* reproduces a quasi-periodic motion with the two incommensurable fundamental frequencies f_1 and f_2 as well as their linear combinations. An increase in the temperature difference leading to a Rayleigh number of $R = 3.3 \times 10^4$ yields a frequency locking with $f_1/f_2 = 7$, i.e. a periodic motion.

In Libchaber's experiments, the velocities were measured with such high precision that it proved possible to confirm Feigenbaum's route to chaos via period doublings quantitatively as well. Figure 20 presents a series of power spectra for increasing Rayleigh numbers. It can be seen from the line spectra that the subharmonics $f_1/2$,

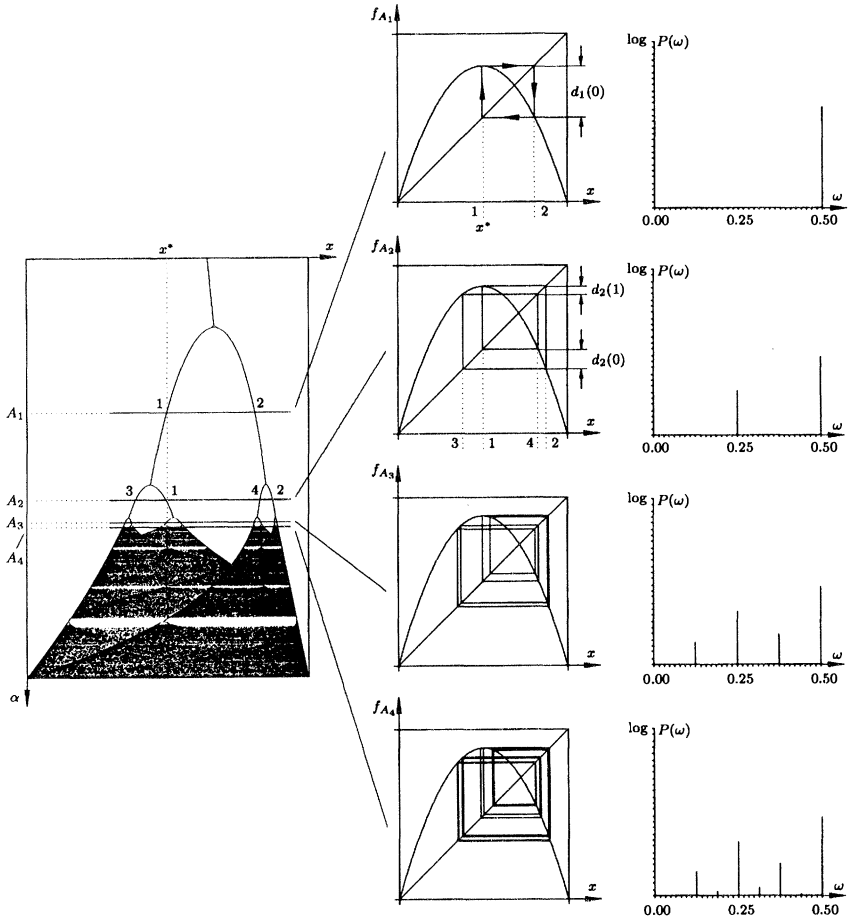

Figure 21. Scaling laws of the superstable cycles and the power spectra for the logistic mapping.

$f_1/4$, $f_1/8$, $f_1/16$ as well as their odd multiples emerge and join the fundamental frequency one after the other. Moreover, the power spectra obey quite special scaling laws which can be unveiled with the aid of the renormalization technique. From figure 20*d* it can be seen that the amplitudes of the subharmonic contributions which emerge sequentially at each period doubling decrease on average by a factor μ^{-1}; according to an estimate of Feigenbaum (1979*b*), μ can be deduced from the Feigenbaum constant a,

$$\mu = \frac{4a}{\sqrt{[2(1+1/a^2)]}} \approx 6.57. \tag{13}$$

In figure 21, we present the corresponding power spectra for the logistic mapping. The scaling of the power spectra results from the banded structure of the 2^k-cycles. A typical Feigenbaum transition from chaos via an inverse cascade of period halving to a single-periodic limit cycle can also be observed in the case of the Lorenz system (2) for $\sigma = 10$, $b = 8/3$ and relative Rayleigh numbers $r > 202$. Figure 22, plate 5, presents phase portraits in the range $330 \geqslant r \geqslant 202$ for decreasing r-values. For $r = 330$, one periodic limit cycle exists which splits into two single-periodic attractors with separate basins of attraction at $r = 233$. These then pass through a cascade of

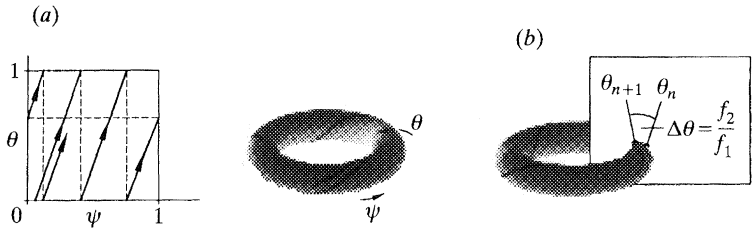

Figure 24. Quasi-periodic motion on a two-dimensional torus with irrational frequency ratio (*a*) and Poincaré section (*b*).

period doublings: for $r = 216$, the period 4 can be seen, for example, and for $r = 215$, period 8. Another reduction of the control parameter r leads to further period doublings in continually decreasing intervals until finally, for $r = 202$, two separate strange attractors appear; interestingly enough, the presence of two strange attractors was not observed before.

The universality of this transition emerges particularly clearly if we plot in dependence of r the Poincaré sections of the Lorenz system generated by cuts with the plane $X = 0$ (see plate 6, figure 23). We obtain a bifurcation diagram which is astonishingly similar to that of the logistic mapping figure 17*a*.

(*d*) *Quasi-periodic transition*

Rand *et al.* (1982) and Shenker (1982), working independently of one another, explored a further transition to chaos. The experimental observations of Gollub & Swinney, for example (figure 14), suggested that there occurs also a direct transition from quasi-periodic to irregular motion. Both groups asked themselves to what extent this transition, like Feigenbaum's period doubling cascade, possesses universal scaling laws. Theoretical investigations based on a simple mapping procedure demonstrated that in this model, the quasi-periodic route to chaos is complementary to Feigenbaum's scenario.

A quasi-periodic motion with two incommensurable frequencies f_1 and f_2 has its equivalent in the phase space in a trajectory on a two-dimensional torus (figure 24*a*) which does not possess a closed path and consequently covers the torus completely. To study the transition to chaos, it is expedient to consider a Poincaré section of the torus (figure 24*b*). In this way, the motion on the torus can be modelled by a simple circle map

$$\theta \to f(\theta) = \theta + \Omega - (K/2\pi)\sin(2\pi\theta) \pmod 1, \tag{14}$$

where K and Ω are control parameters. The parameter K determines the strength of the nonlinearity of the mapping $\theta_{n+1} = f(\theta_n)$. If the nonlinear term vanishes ($K = 0$), $\Omega = \theta_{n+1} - \theta_n = f_2/f_1$ measures the phase shift after one orbit and represents a winding number (figure 14*b*). If $\Omega = p/q$ is rational, the trajectory closes after q orbits and the motion is periodic. Irrational ratios $\Omega = f_2/f_1$ lead to quasi-periodic motions. In the presence of a nonlinear term $(K/2\pi)\sin(2\pi\theta_n)$, the winding number W is defined as the long-term average revolution per iteration

$$W(K, \Omega) = \lim_{n\to\infty} \frac{\theta_n - \theta_0}{n}. \tag{15}$$

For fixed values $K_0 (0 < K_0 < 1)$, periodic motions with a rational winding number are stable over a whole Ω-range. The stable domains of these periodic motions in the (Ω, K)-plane in which frequency locking occurs (i.e. Ω-intervals where $|f'(K_0, \Omega)| \leqslant 1$

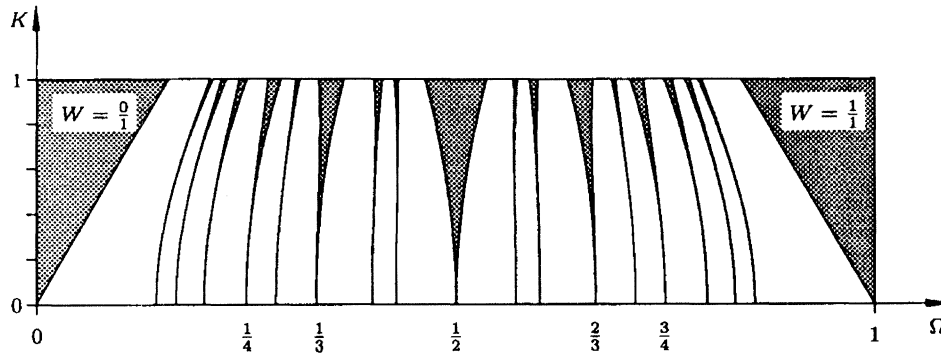

Figure 25. Arnol'd tongues of the circle mapping.

applies) are called Arnol'd tongues (shaded areas in figure 25) (Arnol'd 1965). At every rational value on the Ω-axis, such a periodic window emerges and expands with increasing K. Although there are enumerably infinite resonance horns of this sort with $W = p/q$, they shrink with increasing q so fast that they leave space for quasi-periodic motions. With growing nonlinearity K, however, the probability that frequency locking will occur becomes greater and greater. The value $K = 1$ represents a critical boundary beyond which the circle map is no longer invertible and highly complex long-term behaviour takes place.

In figure 26, plate 6, we plot the Lyapunov exponent σ for the circle map in dependence on the two control parameters Ω and K. Different colours characterize varying long-term behaviour patterns. For negative σ-values, black was chosen: this corresponds to periodic motions respectively fixed points in the Poincaré map. Below the critical boundary $K = 1$, the black Arnol'd tongues can be seen against a dark red background which represents quasi-periodic behaviour ($\sigma = 0$). Beyond the critical boundary, the Arnol'd tongues can overlap. For K-values just beyond 1, the finest tongues overlap first; the broader ones follow for larger K-values. If two Arnol'd tongues with the winding number p/q and p'/q' overlap, the winding number in this (K, Ω)-range is no longer uniquely determined, i.e. depending on the initial condition the orbits are captured by different attractors. Indeed, in this overlap range, there are still infinitely many other Arnol'd tongues with the rational winding numbers $p/q < W < p'/q'$, i.e. there exists an interval of winding numbers.

This representation of the Lyapunov exponent demonstrates that the dynamic behaviour of the circle map becomes increasingly more complex for increasing K-values. Under such conditions, chaotic domains having $\sigma > 0$ can emerge which are depicted in the colours blue-yellow; they in turn are closely interwoven with periodic domains.

In this illustration, the self-similar structure of the Arnol'd tongues can be clearly recognized. Along the line $K = 1$, the Ω-intervals outside the Arnol'd tongues – in which no frequency locking, but quasi-periodic response occurs – form a Cantor set. This suggests a universal scaling law for circle maps at the transition to chaos.

Using the Lyapunov exponents, we can also resolve the detailed structure within the Arnol'd tongues. In figure 27, we show the long-term behaviour of $\theta_n(K)$ (for $\theta_0 = 0.2$) and underneath, the corresponding Lyapunov exponents $\sigma(K)$. A clear similarity to the bifurcation scheme of the logistic map can be observed (figure 17) (θ_n here corresponds to x_n, K to the parameter α). Within the Arnol'd tongues, a route leads evidently to chaos via a cascade of period doublings.

PHILOSOPHICAL TRANSACTIONS OF THE ROYAL SOCIETY A MATHEMATICAL, PHYSICAL & ENGINEERING SCIENCES

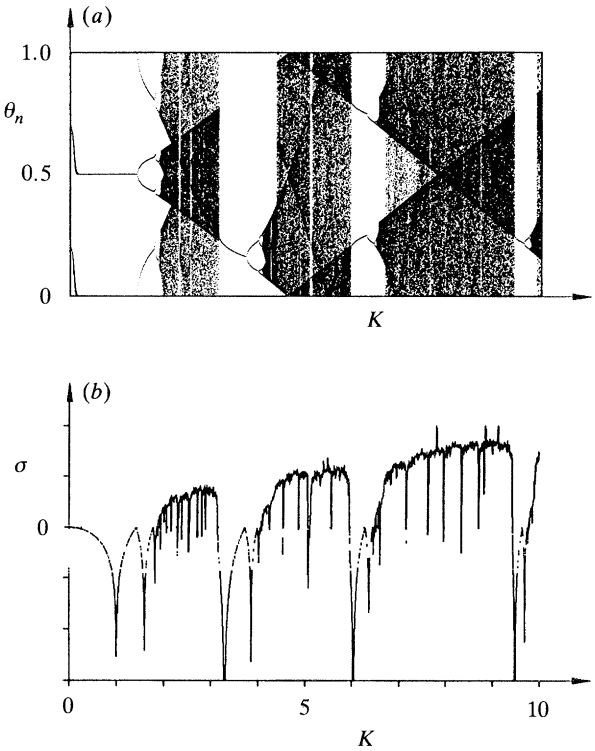

Figure 27. Circle mapping: (*a*) bifurcation diagram and (*b*) Lyapunov exponent within the Arnol'd tongue $W = \frac{1}{2}$ for $\Omega = \frac{1}{2}$.

While for $0 < K < 1$, a whole Ω-range for which the periodic motion is stable appertains to each rational winding number, only a single Ω-value belongs to each irrational winding number. Thus, to discern the direct transition from quasi-periodic behaviour with a fixed winding number to chaos – which is what we are interested in here – two control parameters have evidently to be matched. An increase of the nonlinear coupling, modelled by K, must always be balanced by a shift in Ω in order to exclude a penetration into the Arnol'd tongues (figure 25).

In a series of publications (Rand *et al.* 1982; Ostlund *et al.* 1983; Feigenbaum *et al.* 1982; Shenker 1982) the transition to chaos was studied for a *fixed* irrational winding number (see figure 28). The authors discovered, as in the Feigenbaum scenario, self-similarities that they were able to decode using the renormalization technique. As a winding number, they chose the golden mean $W_G = \frac{1}{2}(\sqrt{5}-1)$ since it can be represented by a particularly simple continued fraction. It later transpired, also from an experimental investigation, that the quasi-periodic transition to chaos is best detected for this particular winding number.

Each irrational number can be represented uniquely by a continued fraction

$$W = \cfrac{1}{n_1 + \cfrac{1}{n_2 + \cfrac{1}{n_3 + \ldots}}} = \langle n_1 n_2 n_3 \ldots \rangle, \tag{16}$$

where the n_i are positive integers. Truncating this fraction after a finite number k of

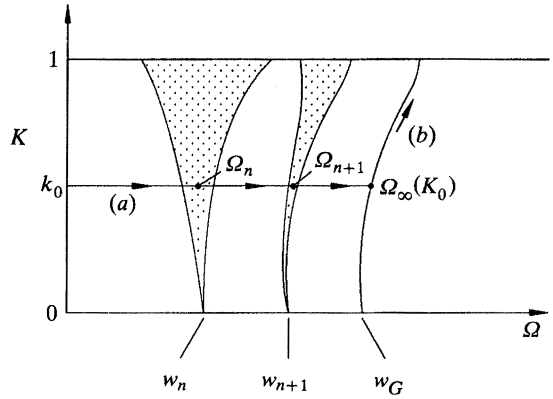

Figure 28. Quasi-periodic transition to chaos with the golden mean $W_G(=\frac{1}{2}(\sqrt{5}-1))$ as the winding number: (*a*) determination of Ω_∞ for $0 < K < 1$, (*b*) transition to limes $K = 1$. $W_n = F_n/F_{n+1}$.

places, we obtain a finite continued fraction which represents a rational number. The 'degree of irrationality' of a number can be characterized by the speed with which the approximation with rational numbers resulting from successive truncations of the continued fraction converges. Rand and Shenker chose the golden mean as the winding number because of its particularly simple continued fraction representation

$$W_G = \langle 1\ 1\ 1 \ldots \rangle = \tfrac{1}{2}(\sqrt{5}-1). \tag{17}$$

Since in this case, the approximation with rational numbers converges at its slowest, W_G is the 'most irrational' of all irrational numbers. Moreover, successive approximations W_n of the golden mean are closely linked with Fibonacci's numbers, F_n, defined by

$$F_{n+1} = F_n + F_{n-1} \quad \text{with} \quad F_0 = 0, \quad F_1 = 1. \tag{18}$$

In fact, we have

$$W_n = F_n/F_{n+1}. \tag{19}$$

As shown in path (*a*) of figure 28, Shenker (1982) approximated for a fixed value $0 < K_0 < 1$ the uniquely determined value $\Omega_\infty(K_0)$ appertaining to the golden mean W_G as the winding number. He considered a series of Arnol'd tongues corresponding to the rational winding numbers $W_n = F_n/F_{n+1}$ $(n = 1, 2, \ldots)$ for which a periodic motion with F_{n+1} cycle points can be observed. For reasons of uniqueness special Ω_n-values have to be selected, for example those for which $\theta = 0$ belongs to the F_{n+1}-cycle. The sequence of these Ω_n-values then tends geometrically towards the limit $\Omega_\infty(K_0)$

$$\lim_{n\to\infty} \frac{\Omega_n - \Omega_{n-1}}{\Omega_{n+1} - \Omega_n} = -\delta. \tag{20}$$

The distances d_n between $\theta = 0$ and the next cycle point also converge geometrically

$$\lim_{n\to\infty} \frac{d_n}{d_{n+1}} = -a. \tag{21}$$

Applying a similar technique to that used for the Feigenbaum scenario, the constants a and δ can be deduced from a fixed point equation applying a suitable iteration operator with the aid of the renormalization theory. Proceeding to the limit $K \to 1$ (path (*b*) in figure 28) and approaching the transition to chaos, we obtain the values

$$a = 1.288575\ldots, \quad \delta = 2.833\,62\ldots. \tag{22}$$

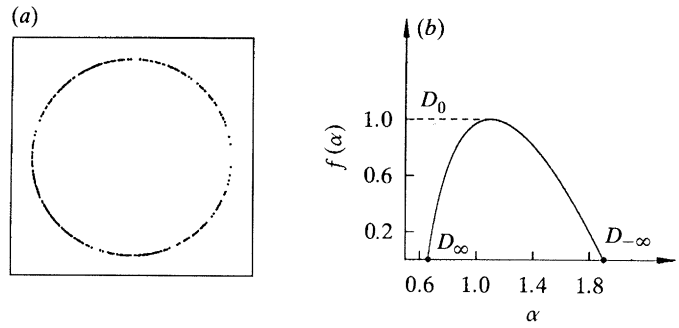

Figure 29. (*a*) Multifractal structure of the attractor of the circle mapping for $K = 1$ with the golden mean as the winding number, (*b*) associated $f(\alpha)$-spectrum (cf. Halsey *et al.* 1986).

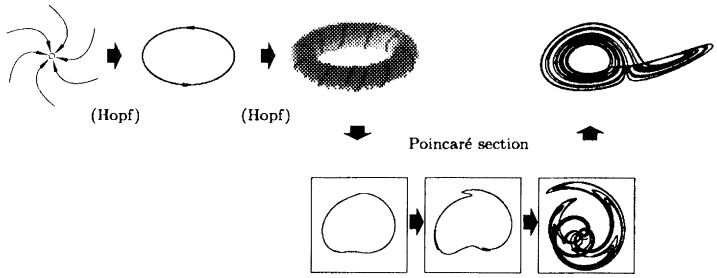

Figure 30. Quasi-periodic transition to chaos.

As in the Feigenbaum scenario, it is important to note that these constants possess once more universal character in the sense that they are independent of the special form of the circle map $\theta_{n+1} = f(\theta_n)$ as long as the latter satisfies only some very weak conditions, for example in that it possesses a cubic inflection point at the critical line ($K = 1$).

As long as $K < 1$, a quasi-periodic motion on a two-dimensional torus corresponds to the circle map for irrational winding numbers. In the Poincaré section, the points of intersection fill a complete circle uniformly. At the transition to chaotic behaviour, however, the characteristics of this Poincaré section change suddenly. In figure 29*a*, we have constructed the critical attractor by iteration of the circle map for the values $K = 1$ and W_G. Although the whole circle is gradually filled, the distribution of the points displays a highly varying density. Since this critical attractor can also be determined experimentally, a characterization of this distribution of density is of interest. Specifying a single dimension so as to reproduce the density pattern of points is certainly not expedient since such a number, as a scalar quantity, cannot describe the inhomogeneous multifractal structure of the set of points. To circumvent this difficulty we use the following device: we cover the attractor with intervals of length l and calculate the probability p_i with which a point falls into the ith interval

$$p_i(l) = l^{\alpha_i(l)}. \tag{23}$$

In the limit $l \to 0$, the scaling index α_i is identical with the point-wise dimension. If one considers now the set of all points with the same α and determines its dimension $f(\alpha)$, we find that f is a universal function which is independent of the special form of the underlying circle map (figure 29*b*).

Figure 30 displays schematically the quasi-periodic transition to chaos which goes hand in hand with the disintegration of the two-dimensional torus. An increase of the

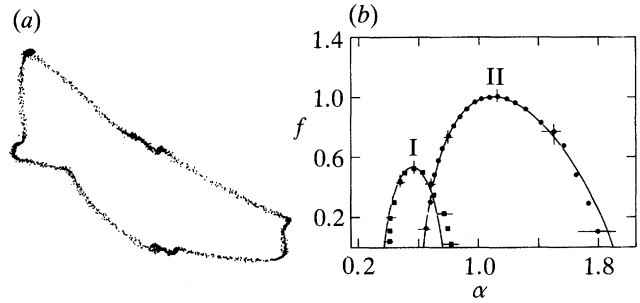

Figure 31. Rayleigh–Bénard experiment: (*a*) critical attractor, (*b*) corresponding $f(\alpha)$-spectrum for a golden mean winding number (curve II). The left curve I shows $f(\alpha)$ for a transition to chaos via period doubling for $W = 8/13$ (Libchaber 1987).

control parameter K causes an increase of the nonlinear term and generally leads to a rise of the effective dimension in the long-term behaviour. Consequently, we have modelled the disintegration of the torus by means of the two-dimensional dissipative circle map

$$\left.\begin{aligned} \theta_{n+1} &= \theta_n + \Omega - (K/2\pi)\sin(2\pi\theta_n) + br_n \pmod 1, \\ r_{n+1} &= br_n - (K/2\pi)\sin(2\pi\theta_n), \end{aligned}\right\} \tag{24}$$

where r_n, θ_n are polar coordinates and b defines a finite rate of dissipation. The wrinkles in the Poincaré section are symptomatic and can also be observed experimentally (cf. figure 31*a*).

Working in the hydrodynamic domain and in particular on an experimental verification of the Rayleigh–Bénard convective flow, Jensen *et al.* (1985) were able to confirm the universal scaling characteristics of the attractor at the transition from quasi-periodic to chaotic behaviour. They used mercury as the fluid to exploit its electrical conductivity. The temperature difference between the plates was adjusted so that the convection rolls oscillated with a given frequency f_1. To generate a second frequency and hence a quasi-periodic motion, an electrical current sheet was passed through the mercury; its amplitude A and frequency f_2 served as control parameters. In the experiment, the transition from quasi-periodic to chaotic behaviour was to be studied for the fixed winding number W_G (cf. figure 28). An increase of the amplitude A causes a more pronounced nonlinear coupling of the two oscillations and thus corresponds to an increase of the parameter K in the circle map. To achieve in the experiment a quasi-periodic motion with the winding number W_G for each fixed A, the ac frequency f_2 had to be adjusted successively in accordance with (19) so that $f_2/f_1 = W_n$ applies. In this way, the scaling laws (20)–(22) could be verified. Figure 31 presents the experimental results at the transition to chaos. In particular, figure 31*a* shows a Poincaré section at the critical boundary. The varying density of the distribution of the points on the attractor is clearly visible. The experimental results yielded the $f(\alpha)$-spectrum of the multifractal structure (figure 31*b*). The measurements (indicated by dots) agree extremely well with the theoretical spectrum as deduced for the circle map (solid line). The right curve II applies to W_G as the winding number, the left curve I to the transition of the period doubling cascade to chaos within an Arnol'd tongue with the winding number $W = 8/13$. With the help of the $f(\alpha)$-spectrum, it proves thus possible to differentiate clearly between the two routes to chaos.

At the transition from quasi-periodic to chaotic behaviour, there occur two types of universality.

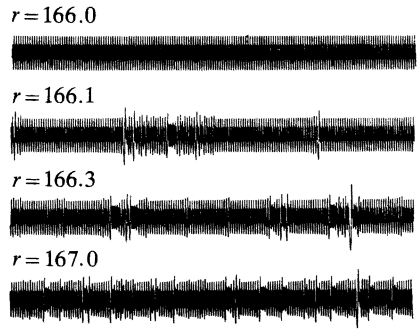

Figure 32. Lorenz system: transition to chaos via intermittency (type I) (Manneville & Pomeau 1979).

Local universality is associated with a fixed winding number W and exhibits close similarities to the scaling behaviour of the period doubling cascade according to Feigenbaum. As the delicate set-up of Libchaber's test shows, however, experimental proof of this scaling laws is difficult since the experiment involves a phase transition in which *two* control parameters have to be matched so that the winding number remains constant.

Global universality, on the other hand, encompasses a whole range of winding numbers and is easier to observe experimentally. The global scaling laws include the self-similar structure of the Arnol'd tongues in which periodic motion occurs; the same observation applies to their complementary set (see figure 26). We have already mentioned that the set of all Ω-values along the critical boundary $K = 1$ appertaining to quasi-periodic behaviour is a Cantor set. Its capacity dimension is a universal quantity and the theoretical value $D_c \approx 0.87$ (Jensen *et al.* 1983) could also be verified experimentally.

(e) *A route to chaos via intermittency*

As a last scenario of a transition to chaos we consider here the route via intermittency, discussed in detail by Pomeau & Manneville (1980). What is intermittency? Intermittency in hydrodynamics expresses that laminar behaviour is interrupted by turbulent outbreaks at irregular intervals. In fact, spatio–temporal intermittency is a well-known phenomenon which can be observed in boundary layers, in pipe flows and in fully developed turbulence.

In the present theory of chaos, the concept of intermittency is restricted to purely temporal processes; it can be confirmed experimentally at the transition from periodic to chaotic behaviour and can also be explained theoretically.

Figure 32 shows various temporal responses of the Lorenz system (2) for an increasing control parameter r. For $r < r_c \sim 166.07$, the long-term behaviour in the phase space is described by a stable limit cycle which loses its stability at r_c. For r-values just above r_c, periodic behaviour can be ascertained over long periods of time; however, it is repeatedly interrupted by chaotic outbreaks at irregular intervals. With increasing r, the regular phases become shorter and shorter until finally, completely irregular behaviour sets in.

Following the theory of bifurcation of fixed points in one-parameter mappings, there are three possibilities for a loss of stability of a periodic motion respectively of a fixed point in the corresponding Poincaré map: an eigenvalue of the mapping matrix of the linearized system crosses the unit circle in the complex λ-plane at $+1$,

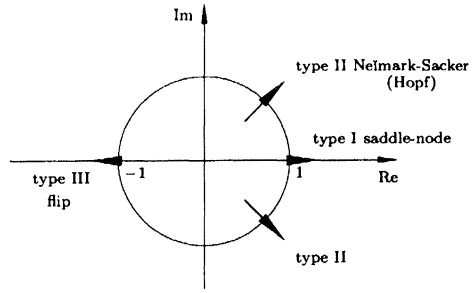

Figure 33. Classification of intermittency on the basis of the eigenvalues.

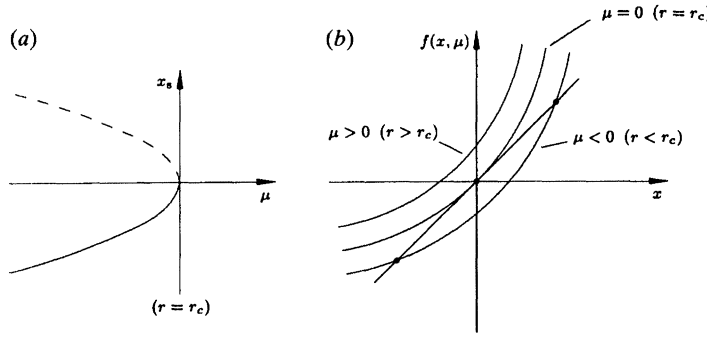

Figure 34. Sub-critical saddle node bifurcation: (*a*) bifurcation diagram, (*b*) mapping function near the bifurcation.

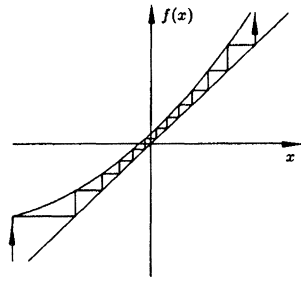

Figure 35. On a laminar phase for an intermittency of type I.

or -1; alternatively, two conjugate complex eigenvalues may cross the circle (figure 33). In the same way, intermittency can be divided into three classes, types I–III. In the case of type I, a saddle-node bifurcation occurs, in the case of type II, a Neĭmark–Sacker bifurcation (Hopf) and in type III, a flip bifurcation (Wiggins 1990); the bifurcations must be sub-critical, however, since intermittency only occurs if the nonlinear effects lead to an increase of the instability.

In the following, we restrict ourselves to a theoretical model for the interpretation of intermittency of type I. In this case, the Poincaré map, as seen in figure 34, experiences a saddle-node bifurcation. Without any loss of generality, we need only consider the normal form of this map for the sub-critical case

$$x \to f(x, \mu) = x + \mu + x^2 \quad \text{with} \quad \mu = (r - r_c)/r_c. \tag{25}$$

For $r < r_c$, a stable and an unstable fixed point exist which merge for $r = r_c$ and vanish for $r > r_c$. In the case of r-values just above r_c, a narrow corridor emerges

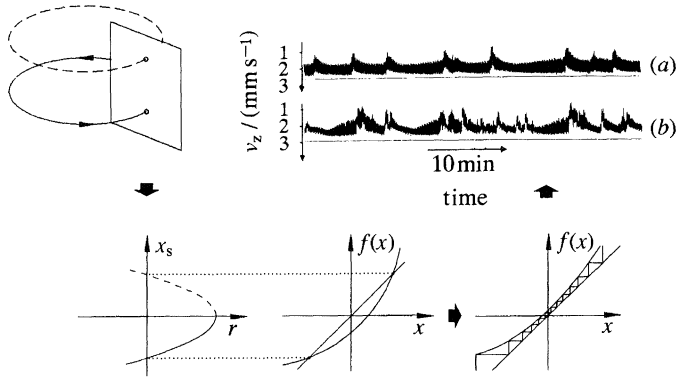

Figure 36. Route to chaos via intermittency of type I. (*a*) $R/R_c = 300$, (*b*) $R/R_c = 335$.

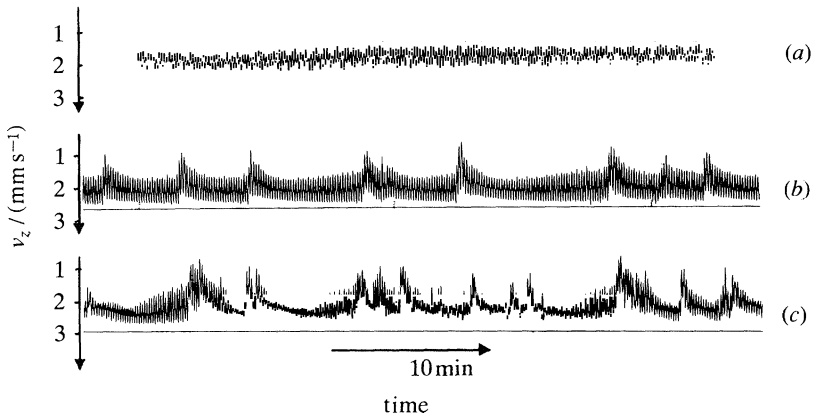

Figure 37. Time-history response of the vertical velocity component for various Rayleigh–Bénard experiments: transition to chaos via intermittency of type I (Bergé *et al.* 1980). (*a*) $R/R_c = 270$, (*b*) $R/R_c = 300$, (*c*) $R/R_c = 335$.

between the curve of the Poincaré map and the first angle bisector (figure 35). Whenever an x-value approaches closely the 'sluice', it traverses the corridor in many small iteration steps. In this range, the response of the motion strongly resembles the stable periodic motion for $r \leqslant r_c$ and generates a laminar phase. Once the tunnel has been passed, an irregular outbreak with increasing amplitudes follows until the orbit is again captured by the sluice. It is relatively easy to deduce a scaling law for the average duration T of the laminar phase

$$T \sim |r - r_c|^{-\frac{1}{2}}. \tag{26}$$

Figure 36 shows this route to chaos via an intermittency of type I. Bergé *et al.* (1980) were able to prove this transition to irregular motion experimentally for the Rayleigh–Bénard convection (figure 37).

3. Remark to the concept of universality

One of the most remarkable findings of the theory of dynamical systems is the concept of universality which is in effect a characteristic of highly dissipative systems. In a manner similar to that used for the classification of bifurcations into a few normal forms, the various transitions from regular to chaotic behaviour can be

grouped in a few scenarios, irrespective of whether the underlying dynamical system describes the dynamics of a mechanical oscillator (Duffing 1918), an electrical circuit (van Buskirk & Jeffries 1985), a chemical reaction, a heart rhythm, the evolution of biological populations (May 1976) or the onset of turbulence in a Bénard cell. As a result of a modification of one (for a direct transition from quasi-periodicity to chaos, two) control parameter(s), nonlinear systems, which are at first not related at all, follow one of the universal instability hierarchies this being also quantitatively provable. Since universal behaviour does not depend on system-specific details, it is possible to predict in this way which transition scenarios are to be expected in an unknown complex system. Although the theory of dynamical systems is still in its infancy both from the theoretical and the practical, numerical point of view, an essential and certainly indispensible first step has been taken on the road to a better comprehension of nonlinear systems.

4. Conclusions and what next?

For more than a century, research work in the engineering sciences has, in general, been directed towards linear systems or linearized ones. In such cases, fundamentally elementary analyses are possible and predictability is guaranteed. It is becoming more and more apparent, however, that linear approximations are nowadays only acceptable to a limited extent in technical and physical applications and that the number of potential fields of application in nonlinear dynamics is growing rapidly on account of their technical relevance.

In mechanics, for example, stability investigations of externally excited systems are of major significance. In particular, we are confronted by complex nonlinear problems like the anchorage of oil rigs in heavy sea, boat capsizing, the behaviour of coupled systems such as lorry and trailer, not to forget the stability of satellites as well as of the moons of some planets in our solar system. Also, in hydrodynamics, stability investigations of multi-phase and convection flows are the object of lively research.

The greatest hope physicists have been fostering since the beginning of research in chaos is to gain a deeper physical understanding of turbulent behaviour and to invent new associated computational devices. 'Indeed, if one had to choose just one ''most important'' area of future studies of chaos, it would have to be the relationship between chaos and turbulence' (Campbell 1987).

The fact that the chaos theory is by now so well established in many scientific fields is undoubtedly based on the quantitative confirmation of its theoretical statements by precise and delicate experiments on the onset of turbulence as carried out by Libchaber and Maurer in experiments on the Bénard convection.

It must be admitted, however, that the limits of the current chaos theory, which is presently centred on temporal evolutions in the dynamics of low-dimensional systems, are gradually becoming apparent. In the aforementioned Rayleigh–Bénard experiments, a great effort had to be applied to freeze the spatial modes. In fully developed turbulence, however, spatially disordered structures are generated in addition to temporal irregularities on (at least apparently so) all scales; these scales are reflected in the spatial and temporal broad band power spectra. This entails a drastic increase in the active degrees of freedom and thus a very high dimension of the underlying phase space. In this sense, the standard chaos theory of today is undoubtedly a long way from offering an understanding of fully developed

PHILOSOPHICAL TRANSACTIONS OF THE ROYAL SOCIETY A MATHEMATICAL, PHYSICAL & ENGINEERING SCIENCES

turbulence. On the other hand, numerical and experimental investigations of weak turbulence confirm that turbulence displays all the symptoms of the chaos syndrome and that thus, the theory of dynamical systems seems to be an indispensible tool for the comprehension of the initiation of turbulent motion respectively of the dynamics of general complex systems.

What then are the next steps on the road to comprehending turbulence and combustion, an additional complex field demanding intense research? The strategy will be to attain a gradual unfreezing of the spatial modes. In addition to the bifurcation of purely temporal processes, the occurrence of spatial patterns is a result of spatial instabilities. In open flows, for example, this leads to an increase of the perturbations and to spatial unpredictabilities downstream. This spatial expansion of fluctuations corresponds to a spatial transport of information and is a new additional mechanism.

In future studies, our aim should be to achieve a reduction of the number of modes necessary to model the fundamental characteristics – like spatio-temporal patterns and the transport of energy, mass, concentration – to a minimum. A further important aspect is the elucidation of the creation of self-similar structures by means of iterative processes or hierarchies of equations.

The computer will doubtless play an important role on all investigative levels in the search for the link between chaos and turbulence. Numerical simulations and graphic representations of the results are indispensible aids for the recognition of the internal constraints in dynamical processes. To explore such open problems, we hope that the cellular automata/lattice gas automata will offer new opportunities to simulate on the computer nonlinear dynamical processes with very many degrees of freedom, e.g. liquids at high Reynolds numbers, and perhaps to obtain a better physical understanding.

Thanks are extended by the authors to Harald Volz and Bernd Lehle for the exceptional standard of their graphical contributions. The layout of the manuscript text and figures was prepared, as usual, with immaculate precision by Christiane Reisert.

References

Arnol'd, V. I. 1965 Small denominators I, Mappings of the circumference onto itself. *Trans. Am. Math. Soc.* **46**, 213–284.

Bergé, P., Dubois, M., Manneville, P. & Pomeau, Y. 1980 Intermittency in Rayleigh–Bénard convection. *J. Phys. Lett., Paris* **41**, 341–345.

Bergé, P., Pomeau, Y. & Vidal, Ch. 1984 *Order within chaos: towards a deterministic approach to turbulence*. Paris: Hermann.

Buskirk, van R. & Jeffries, C. 1985 Observation of chaotic dynamics of coupled nonlinear oscillators. *Phys. Rev.* A **31**, 3332–3357.

Campbell, D. 1987 Chaos: chto delat? In *Chaos '87* (ed. M. Duong-Van), Nuclear Physics B (Proc. Suppl.) 2, pp. 541–562. Amsterdam: North-Holland.

Duffing, G. 1918 *Erzwungene Schwingungen bei veränderlicher Eigenfrequenz und ihre technische Bedeutung*. Braunschweig: Vieweg.

Feigenbaum, M. J. 1979*a* The universal metric properties of nonlinear transformations. *J. statist. Phys.* **21**, 669–706.

Feigenbaum, M. J. 1979*b* The onset spectrum of turbulence. *Phys. Lett.* A **74**, 375–378.

Feigenbaum, M. J., Kadanoff, L. P. & Shenker, S. J. 1982 Quasiperiodicity in dissipative systems: a renormalization group analysis. *Physica* D **5**, 370–386.

Gollub, J. P. & Swinney, H. L. 1975 Onset of turbulence in a rotating fluid. *Phys. Rev. Lett.* **35**, 927–930.

Grossmann, S. 1990 Turbulenz: Verstehen wir endlich dieses nichtlineare Phänomen? *Phys.* Bl. **46**, 2–7.

Guckenheimer, J. & Holmes, P. 1983 *Nonlinear oscillations, dynamical systems, and bifurcations of vector fields*. New York: Springer.

Halsey, T. C., Jensen, M. H., Kadanoff, L. P., Procaccia, I. & Shraiman, B. I. 1986 Fractal measures and their singularities: the characterization of strange sets. *Phys. Rev.* A **33**, 1141–1151.

Hénon, M. 1976 A two-dimensional mapping with a strange attractor. *Commun. Math. Phys.* **50**, 69–77.

Hentschel, H. G. E. & Procaccia, I. 1983 The infinite number of generalized dimensions of fractals and strange attractors. *Physica* D **8**, 435–444.

Hopf, E. 1942 Abzweigung einer periodischen Lösung von einer stationären Lösung eines Differentialsystems. *Ber. Math.-Phys. Sächs. Akad. d. Wiss. Leipzig*, **94**, 1–22.

Jensen, M. H., Bak, P. & Bohr, T. 1983 Complete devil's staircase, fractal dimension, and universality of mode-locking structure in the circle map. *Phys. Rev. Lett.* **50**, 1637–1639.

Jensen, M. H., Kadanoff, L. P., Libchaber, A., Procaccia, I. & Stavans, J. 1985 Global universality at the onset of chaos: results of a forced Rayleigh–Bénard experiment. *Phys. Rev. Lett.* **55**, 2798–2801.

Kolmogorov, A. N. 1941 The local structure of turbulence in incompressible viscous fluid for very large Reynolds number. *Dokl. Acad. Sci. SSSR* **30**, 301–305.

Landau, L. D. 1944 On the problem of turbulence. *Dokl. Acad. Sci. SSSR* **44**, 311.

Libchaber, A. & Maurer, J. 1980 Une expérience de Rayleigh–Bénard de géometrie réduite; multiplication, accrochage et démultiplication de fréquences. *J. Phys., Paris* C **341**, 51–56.

Libchaber, A. 1987 From chaos to turbulence in Bénard convection. *Proc. R. Soc. Lond.* A **413**, 63–69.

Lipowsky, R. 1983 Die Renormierung in der statistischen Physik. *Phys. Bl.* **39**, 387–393.

Lorenz, E. N. 1963 Deterministic non-periodic flow. *J. atmos. Sci.* **20**, 130–141.

Malraison, B., Atten, P., Bergé, P. & Dubois, M. 1983 Dimension d'attracteurs étranges: une détermination expérimentale en régime chaotique de deux systèmes convectifs. *C. r. Séanc. Acad. Sci., Paris* C **297**, 209–214.

Manneville, P. & Pomeau, Y. 1979 Intermittency and the Lorenz model. *Phys. Lett.* A **75**, 1–2.

Maurer, J. & Libchaber, A. 1979 Rayleigh–Bénard experiment in liquid helium: frequency locking and the onset of turbulence. *J. Phys. Lett., Paris* **40**, 419–423.

May, R. M. 1976 Simple mathematical models with very complicated dynamics. *Nature, Lond.* **261**, 459–467.

Ostlund, S., Rand, D., Sethna, J. & Siggia, E. 1983 Universal properties of the transition from quasi-periodicity to chaos in dissipative systems. *Physica* D **8**, 303–342.

Packard, N. H., Crutchfield, J. P., Farmer, J. D. & Shaw, R. S. 1980 Geometry from a time series. *Phys. Rev. Lett.* **45**, 712–716.

Pomeau, Y. & Manneville, P. 1980 Intermittent transition to turbulence in dissipative dynamical systems. *Commun. Math. Phys.* **74**, 189–197.

Rand, D., Ostlund, S., Sethna, J. & Siggia, E. D. 1982 Universal transition from quasiperiodicity to chaos in dissipative systems. *Phys. Rev. Lett.* **49**, 132–135.

Ruelle, D. & Takens, F. 1971 On the nature of turbulence. *Commun. Math. Phys.* **20**, 167–192.

Schuster, H. G. 1988 *Deterministic chaos, an introduction*. Weinheim: VHC Verlagsgesellschaft.

Shenker, S. J. 1982 Scaling behavior in a map of a circle onto itself: empirical results. *Physica* D **5**, 405–411.

Sparrow, C. 1982 *The Lorenz equations: bifurcations, chaos and strange attractors*. New York: Springer.

Swinney, H. L. & Gollub, J. P. 1978 The transition to turbulence. *Phys. Today* **31** (8), 41–49.

Takens, F. 1981 Detecting strange attractors in turbulence. In *Lecture notes in Math.*, vol. 898, pp. 366–381. Berlin: Springer.

Wiggins, S. 1988 *Global bifurcations and chaos*. New York: Springer.

PHILOSOPHICAL TRANSACTIONS OF THE ROYAL SOCIETY A MATHEMATICAL, PHYSICAL & ENGINEERING SCIENCES

Wiggins, S. 1990 *Introduction to applied nonlinear dynamical systems and chaos.* New York: Springer.

Wilson, K. G. 1971 Renormalization group and critical phenomena. I. Renormalization group and the Kadanoff scaling picture. *Phys. Rev.* B **4**, 3174–3183.

Received 4 November 1991; accepted 12 May 1992

PHILOSOPHICAL TRANSACTIONS OF THE ROYAL SOCIETY A MATHEMATICAL, PHYSICAL & ENGINEERING SCIENCES

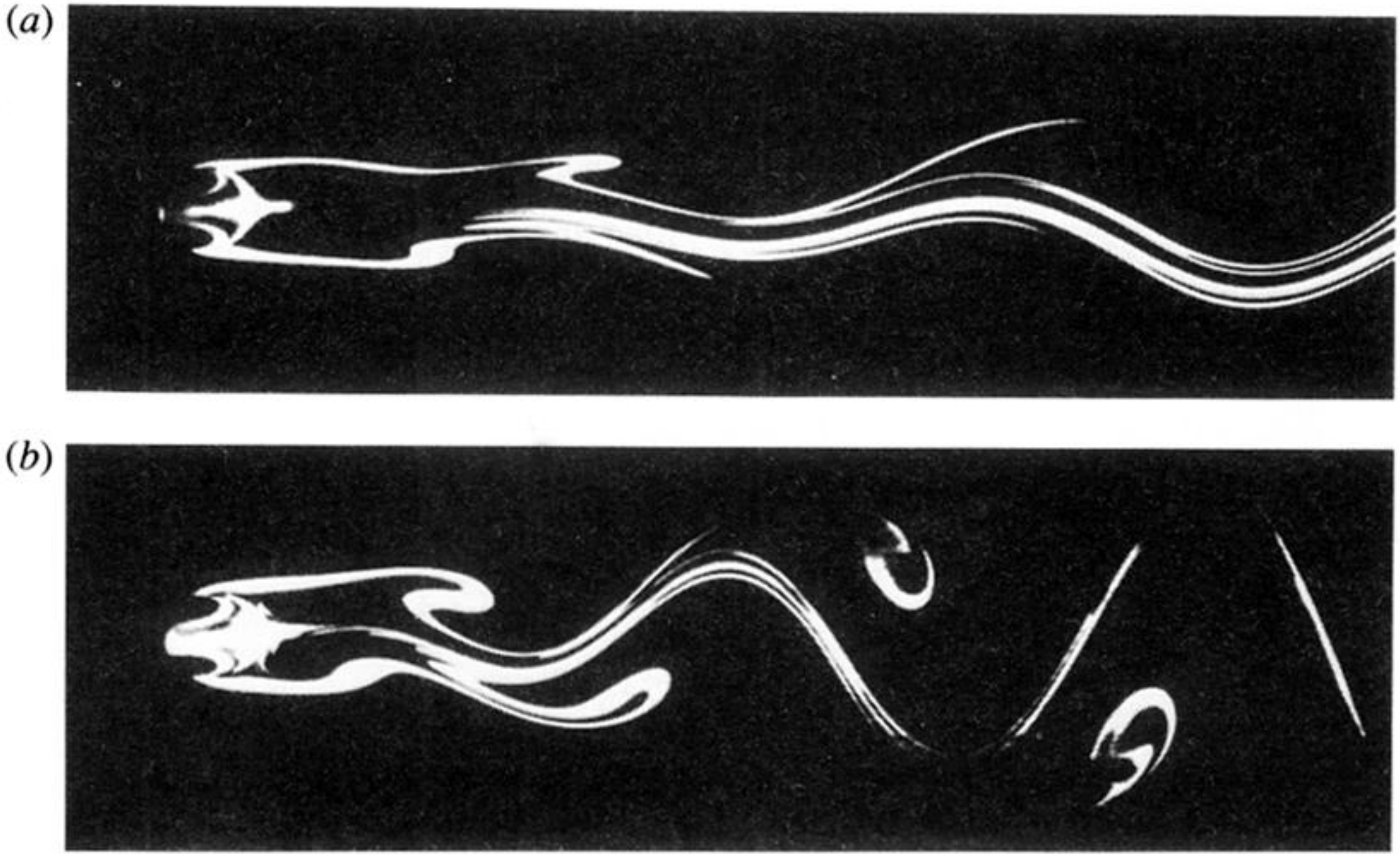

igure 1. von Kàrmàn vortex street, stretching and folding (cf. Bergé *et al.* 1984).

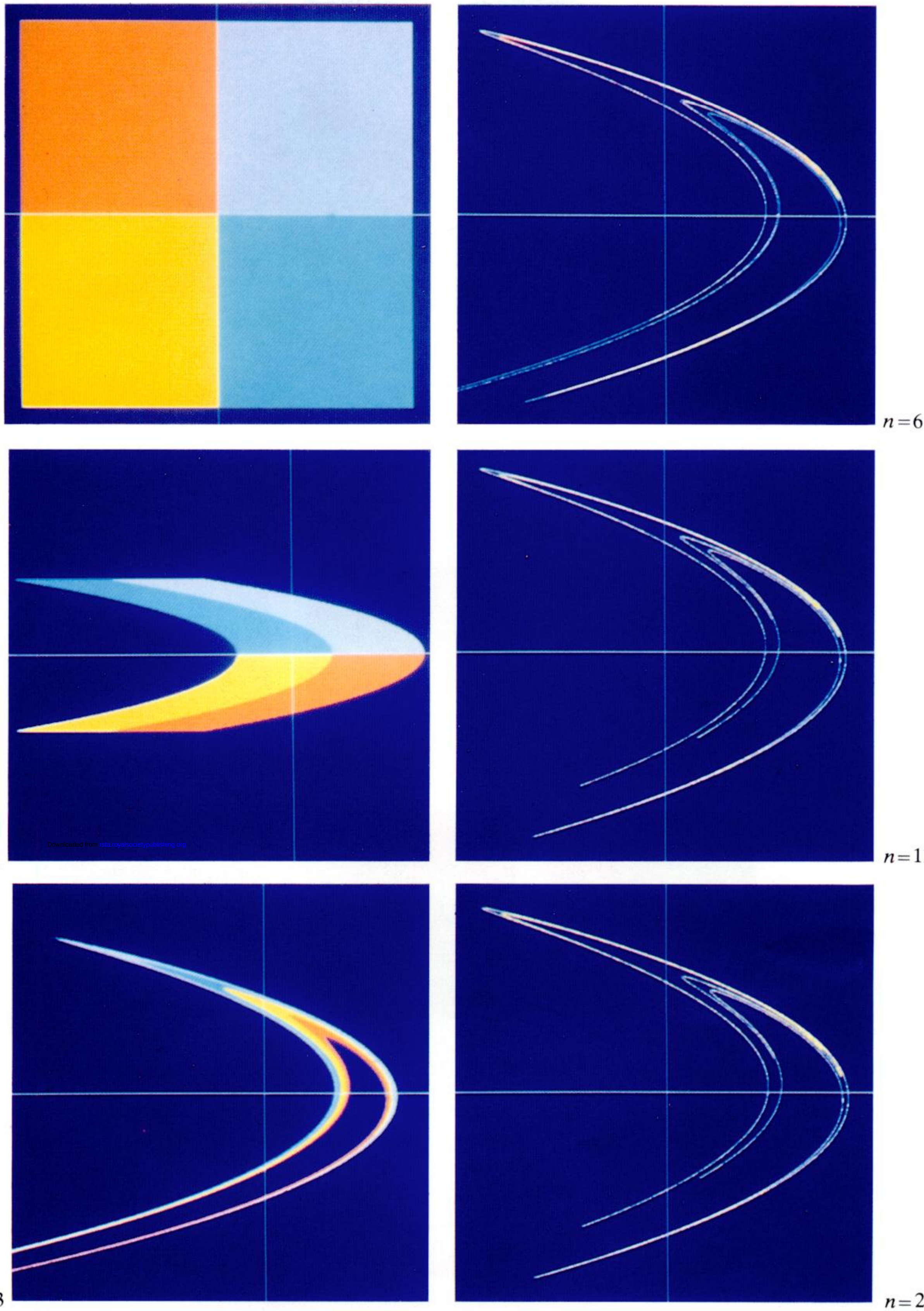

Figure 3. Formation of the Hénon attractor: initial conditions ($n = 0$) assigned to four coloured areas; complete mixing after $n = 29$ iterations.

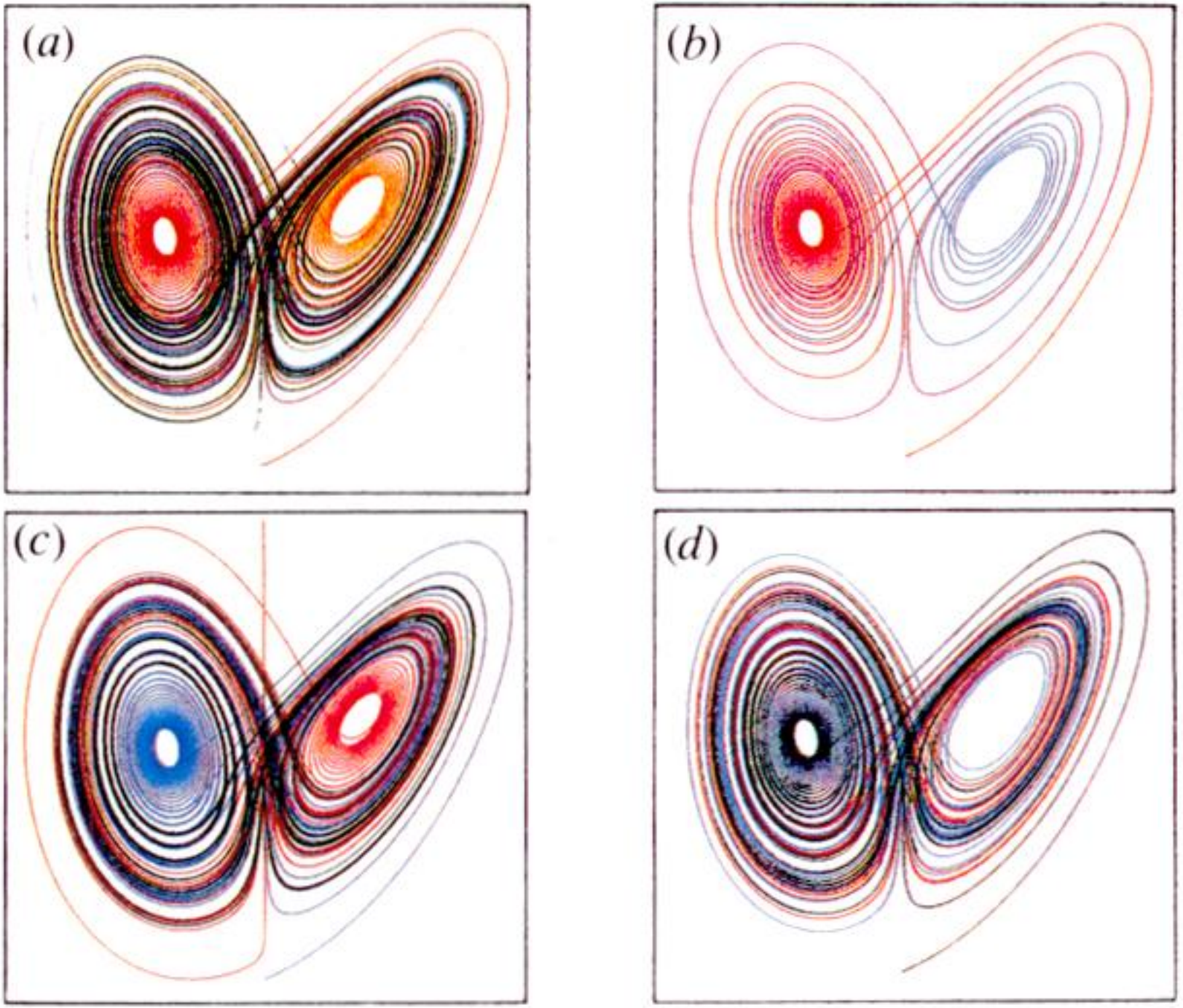

gure 5. Lorenz attractor for $r = 28$, $\sigma = 10$, $b = 8/3$. (*a*), (*b*) Unpredictable jumps, (*c*) basin of attraction, (*d*) sensitive dependence upon initial conditions.

PHILOSOPHICAL TRANSACTIONS OF THE ROYAL SOCIETY A MATHEMATICAL, PHYSICAL & ENGINEERING SCIENCES

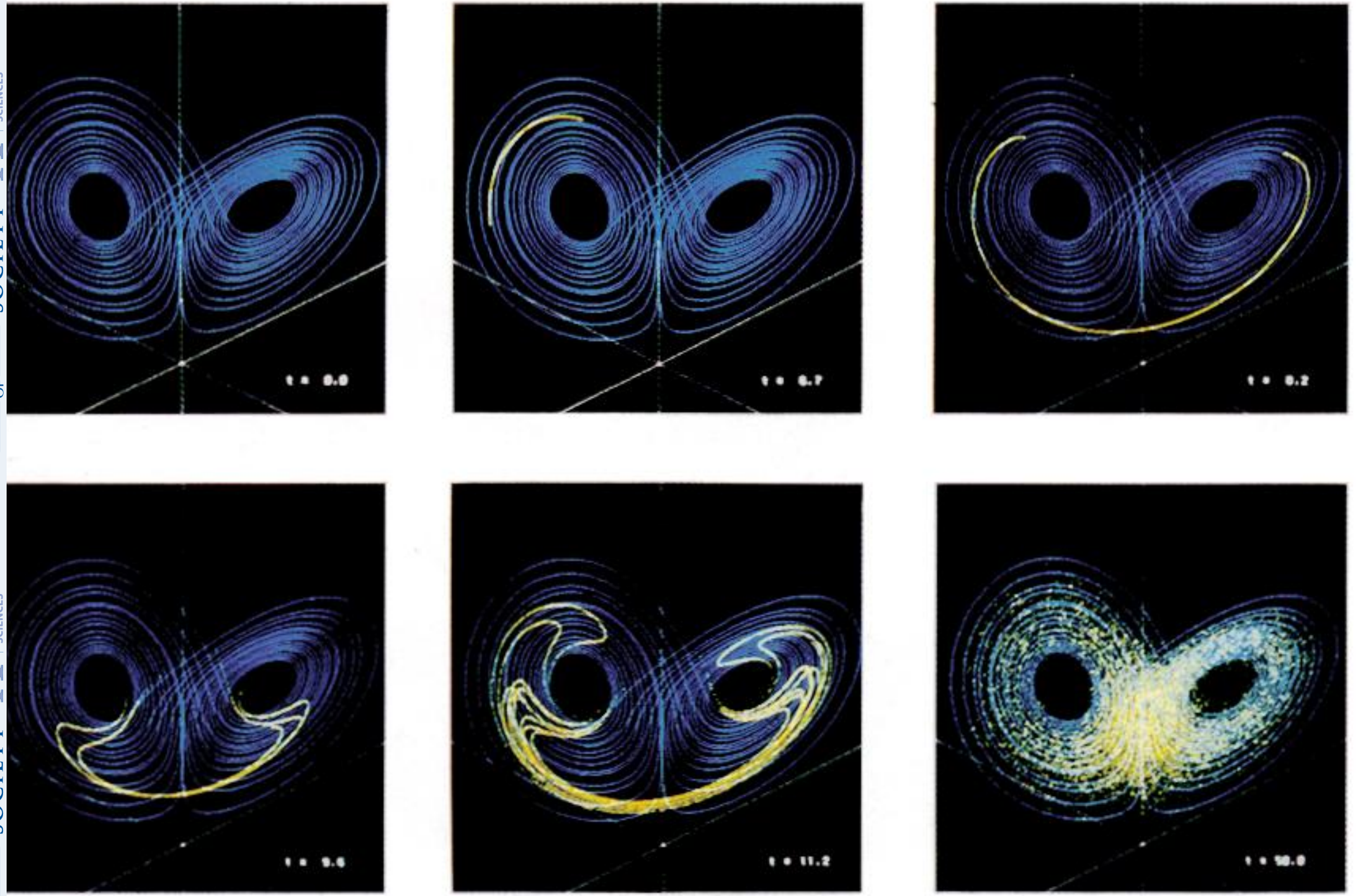

Figure 6. Divergence of neighbouring trajectories.

PHILOSOPHICAL TRANSACTIONS OF THE ROYAL SOCIETY A MATHEMATICAL, PHYSICAL & ENGINEERING SCIENCES

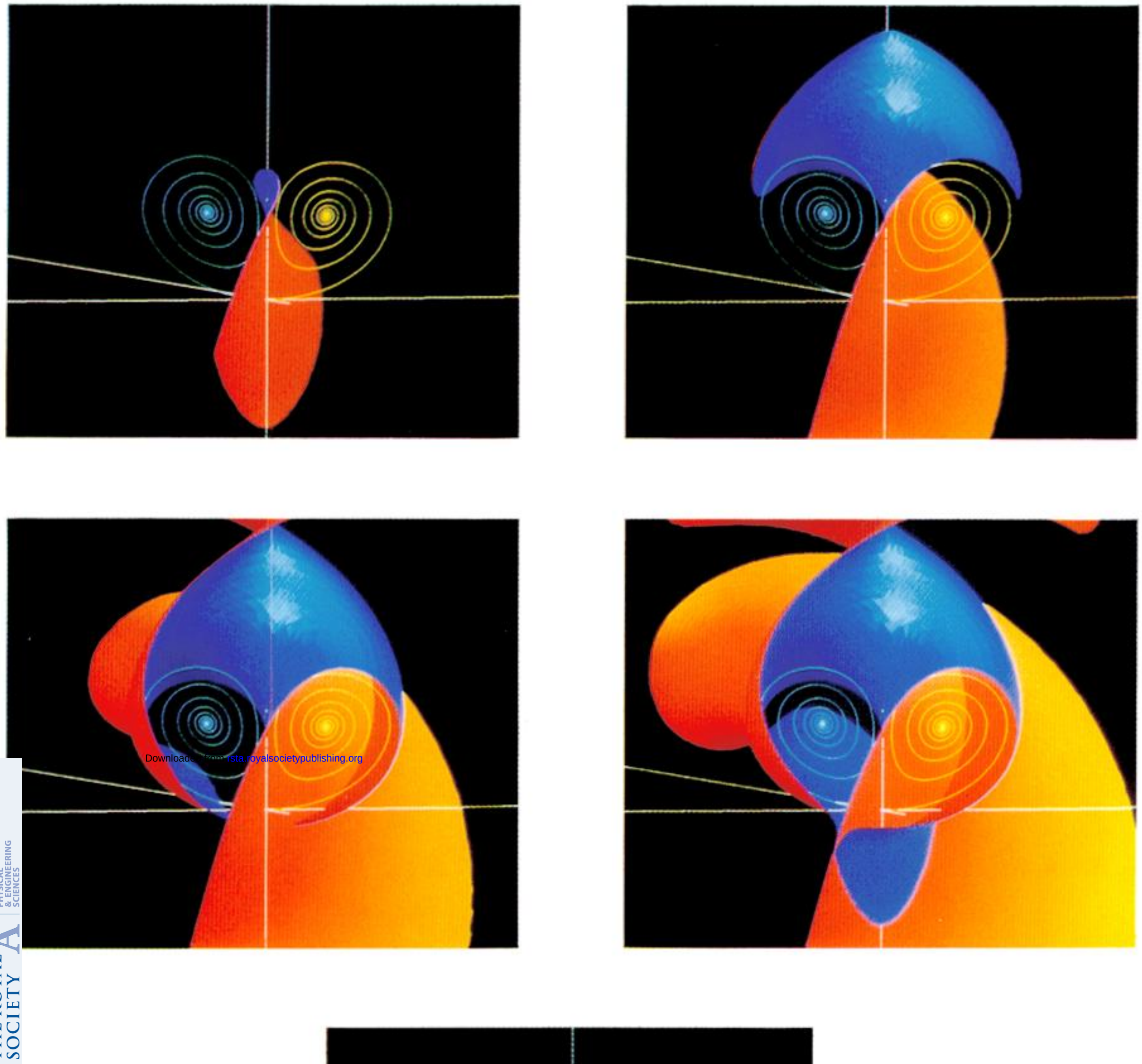

Figure 8. Evolution of the stable manifold (surface) and the unstable manifold (line) appertaining to a fixed point in the origin ($r = 12$).

PHILOSOPHICAL TRANSACTIONS OF THE ROYAL SOCIETY A MATHEMATICAL, PHYSICAL & ENGINEERING SCIENCES

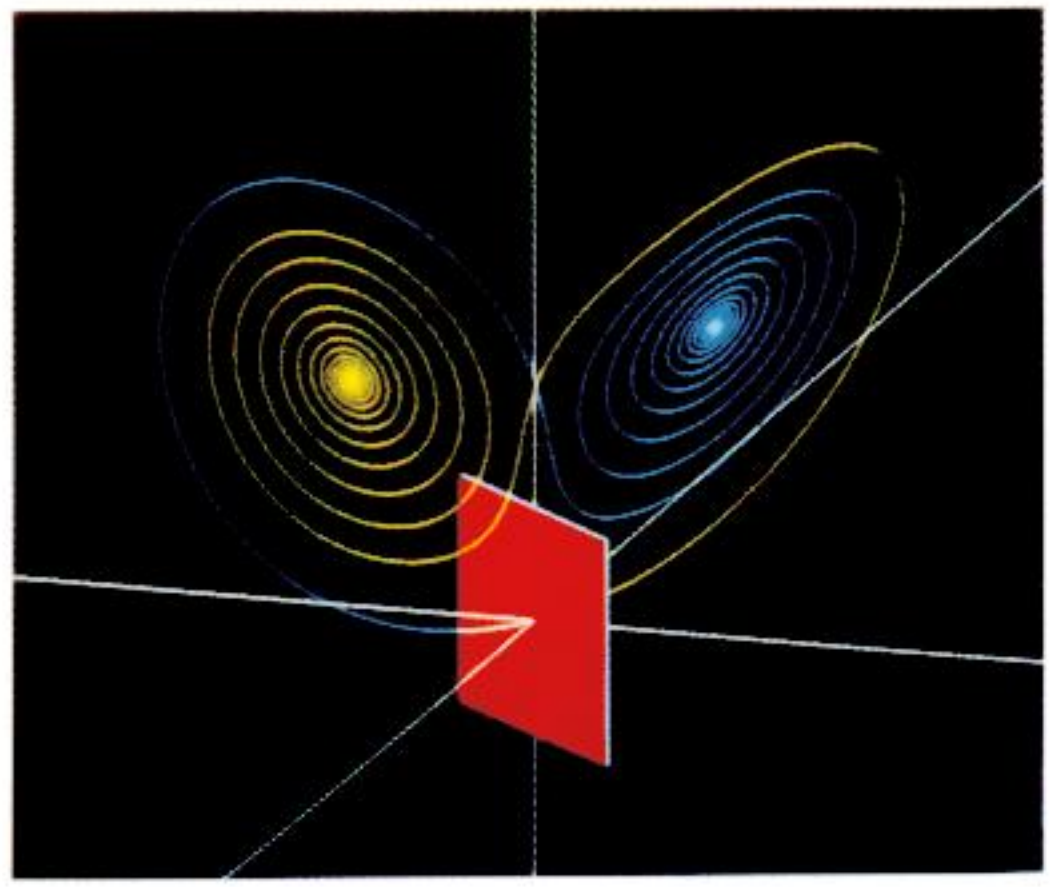

Figure 9. Evolution of the stable manifold (surface) and the unstable manifold (line) appertaining to a fixed point in the origin ($r = 15$).

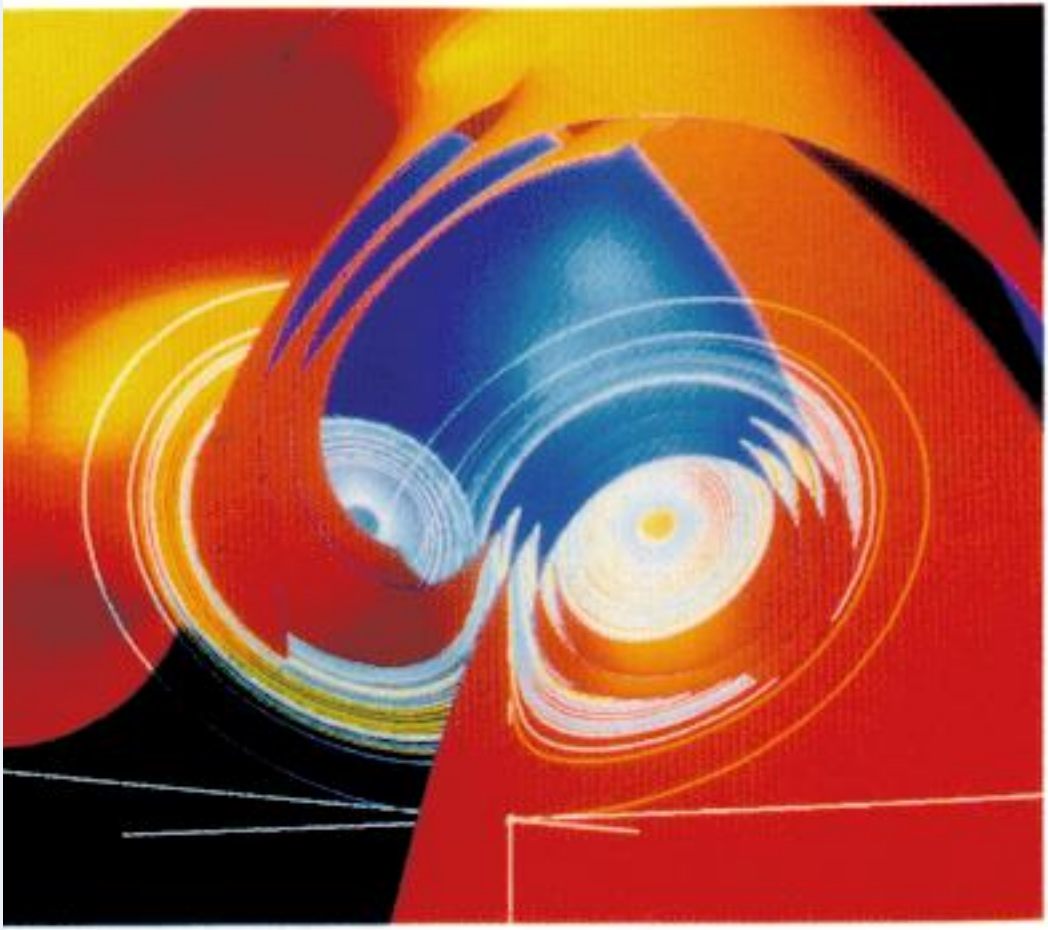

igure 10. Lorenz attractor ($r = 28$).

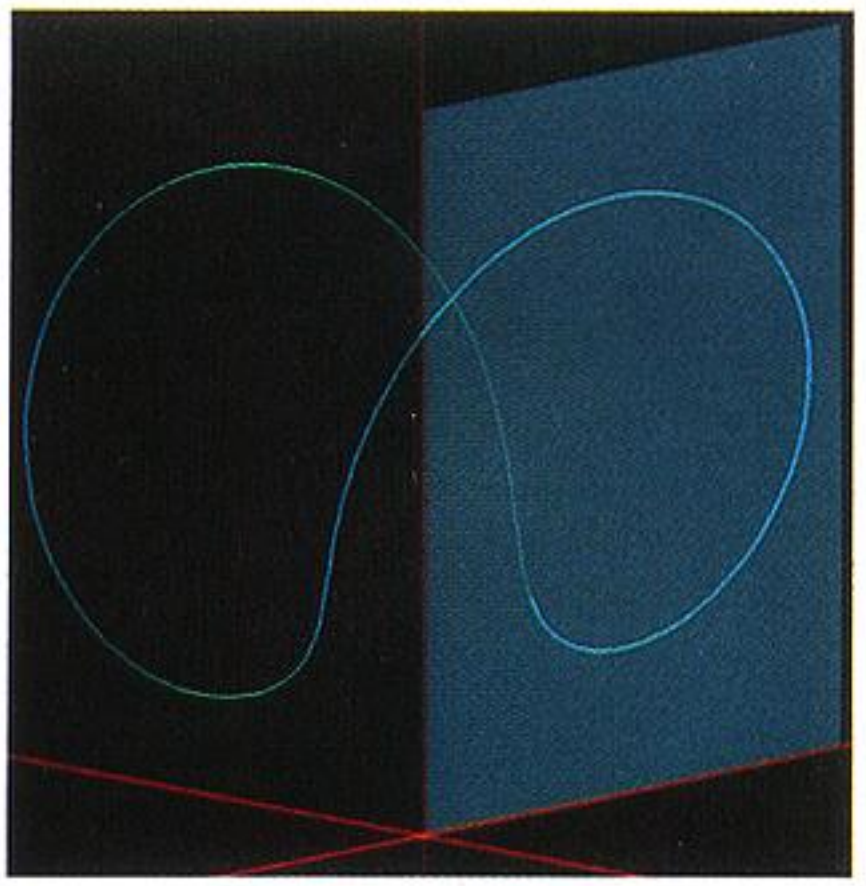

$r = 330$

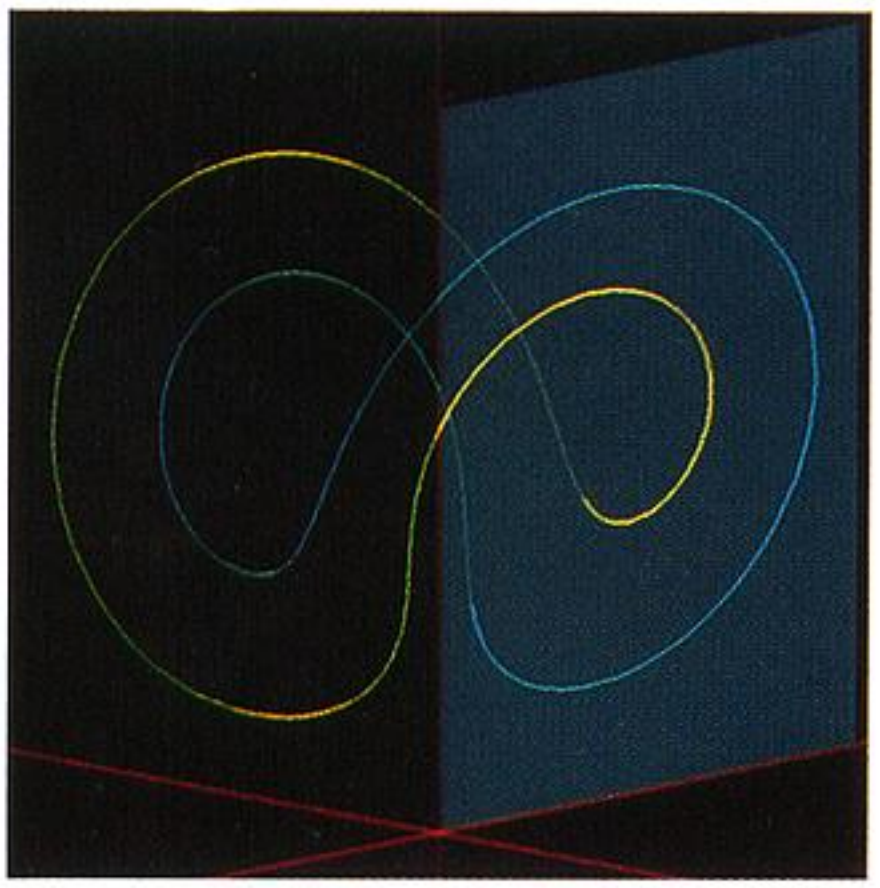

$r = 233$

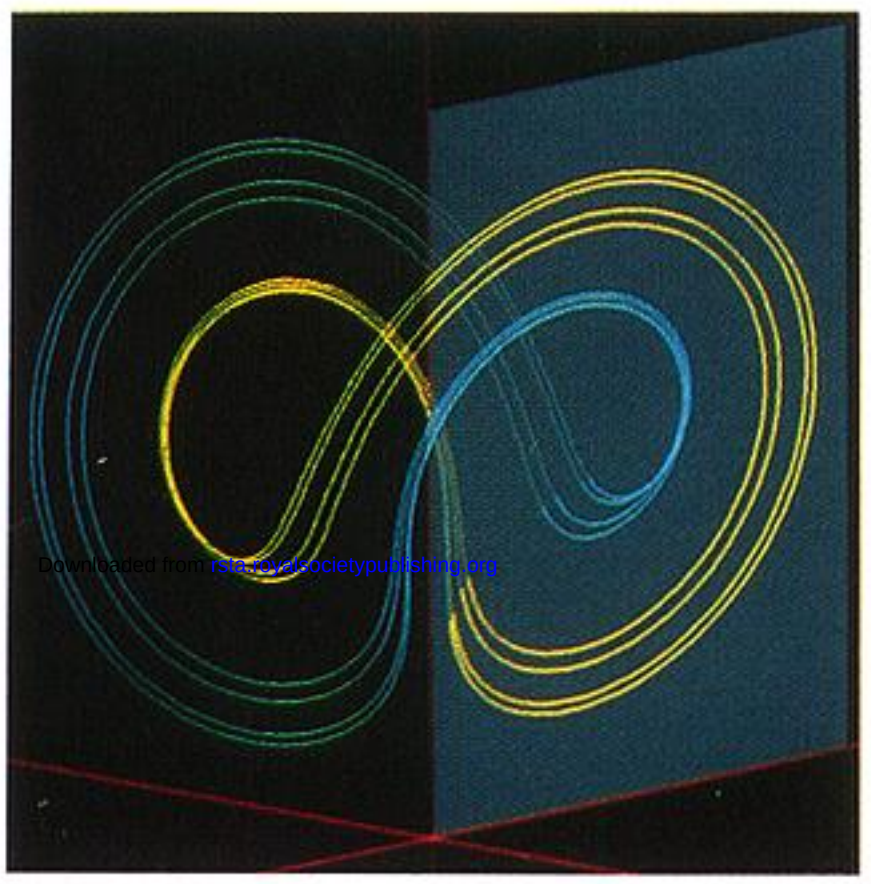

$= 216$

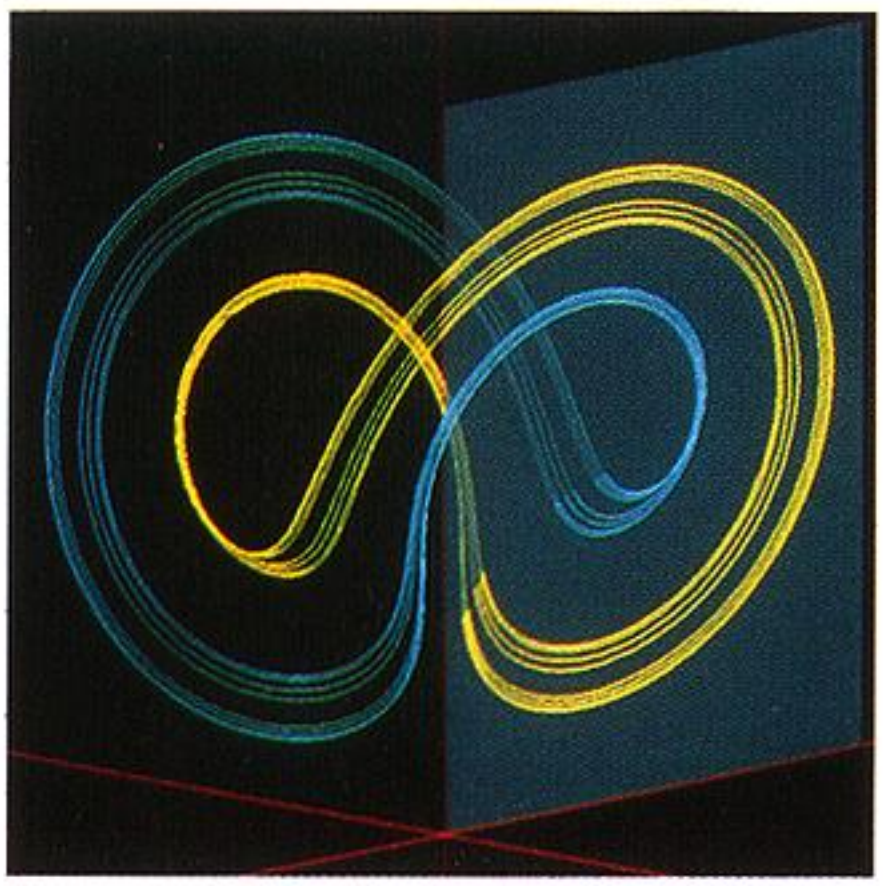

$r = 215$

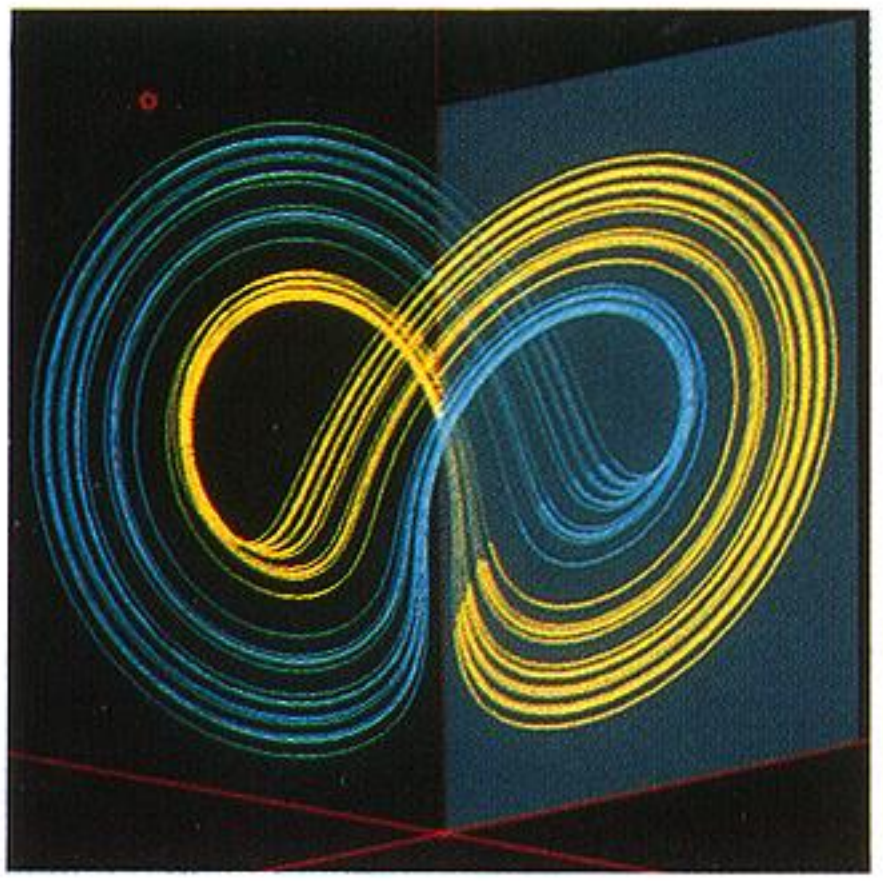

$= 204$

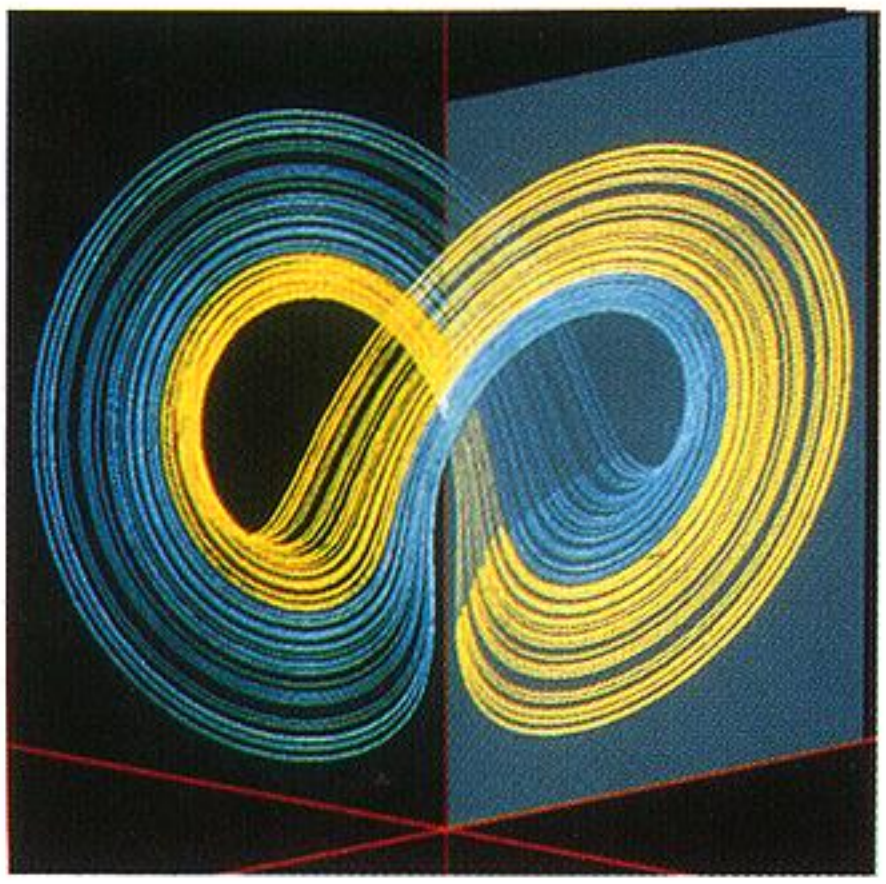

$r = 202$

Figure 22. Lorenz system: co-existence of two attractors and inverse cascade of period doublings.

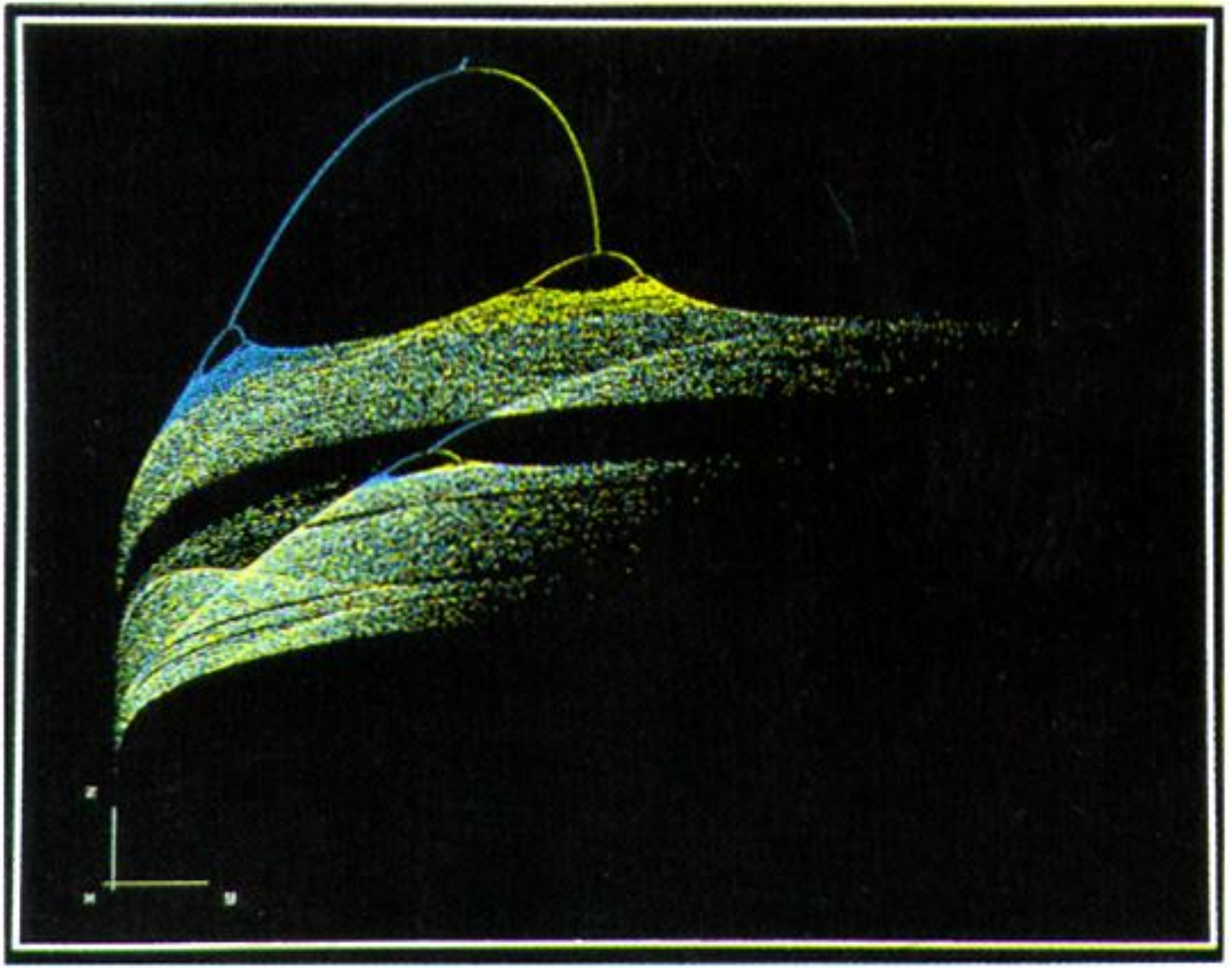

Figure 23. Bifurcation diagram of the Poincaré sections of the Lorenz system for $25 \leqslant r \leqslant 325$.

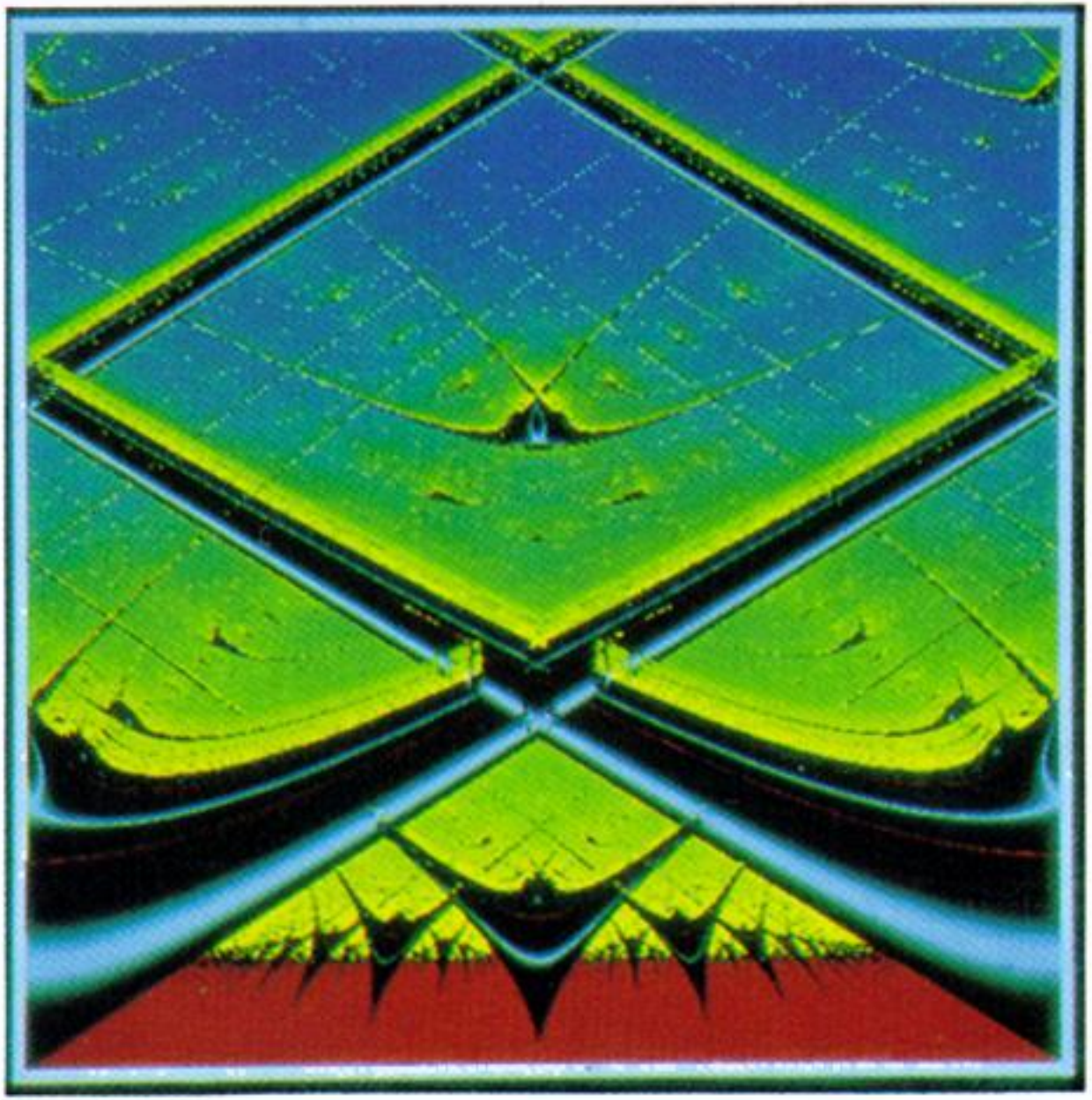

Figure 26. Lyapunov exponent $\sigma(\Omega, K)$ for the circle mapping $(0 \leqslant \Omega \leqslant 1, 0 \leqslant K \leqslant 10)$.